5

ELECTROMAGNETIC FIELD ANALYSIS FOR ELECTRICAL MACHINE DESIGN

M. V. K. Chari, G. Bedrosian, J. D'Angelo, A. Konrad, G. M. Cotzas, and M. R. Shah

5.1 Introduction

Design optimization for high power density electrical machinery at low cost with a high degree of reliability in operation requires accurate performance prediction at the design stage. This in turn requires the

determination of the magnetic field distribution in detail in the machine geometry. The finite-element method offers an efficient and accurate means of performing this task, taking full account of nonlinearity of the iron material; and induced currents in electrically conducting parts. This method requires the formulation of the field problem in terms of partial differential equations expressed in variational terms or by means of a weighted residual function. In the former, an energy-related expression called a functional is minimized with respect to a set of trial solutions. This chapter describes the application of the finite-element method for magnetic field analysis to aid in the design of electrical machinery and devices with distributed material properties and excitation sources. Some of the applications described include utility generators, transformer windings with skin effect, eddy-current loss determination in busbars, and others.

With increasing demand for high power densities, optimal efficiency, low cost, and operational reliability of electrical plant and machinery, it is imperative that accurate and sophisticated methods are employed for improved performance prediction during the design process. Some of the performance indicators of interest to the designer are excitation requirements on no-load and full-load conditions, reactances, transient characteristics, short-circuit forces, iron and stray load losses, end-region fields, eddy-current effects in conducting parts, dielectric stresses in insulating materials etc.

In order that these parameters are evaluated with the desired degree of precision, one must accurately and in detail predict the electric and magnetic fields produced under various operating conditions. Closed from analysis methods [1] and analog techniques [2] have been found to be of limited use and application to simplified geometries and boundary conditions. The need for improved analysis techniques was, therefore, recognized even in the early days of electrical machine design. With the advent of digital computers, numerical methods have become popular and are proving effective for determining the field distribution in electrical apparatus. Some of these currently used methods fall into three principal categories: (i) divided difference schemes [3], (ii) finite-element methods based on projective and variational formulations [4, 5] and (iii) integral equation techniques [6]. Many variants of the foregoing and hybrid methods have also appeared in the technical literature. All of the above methods address the electric and magnetic field problems in terms of mathematical models, their solution, and

processing of the results to obtain design parameters.

The term modeling in this context refers to the formulation of the physical problem in mathematical terms from Maxwell's equations and obtaining the relevant differential or integral expression which describe the inherent electromagnetic relationships. The solution step consists of finding an approximation to the true solution which satisfies these equations so as to minimize the error in a prescribed or acceptable sense. Several approaches are possible for the choice of the solution approximation and the error norm.

This chapter describes (i) the method of modeling the electromagnetic field problem in terms of potential functions, (ii) the derivation of the governing partial differential equations, (iii) the subdivision of the field region into finite elements, (iv) the construction of an approximate solution in terms of interpolatory basis functions, (v) the setting up of an error norm by variational methods and (vi) minimizing the error in a least squared sense to obtain the potential solution.

The principal differential equations considered in this chapter for modeling purposes are: (i) vector Poisson equation for linear and nonlinear magnetostatic problems, (ii) diffusion equation representative of steady-state or transient eddy-current and skin-effect problems, and (iii) scalar Poisson equation for permanent magnet fields. The geometries modeled include two-dimensional, axisymmetric, and three-dimensional representations of the field region. A second-order method of quasi-linearizing the nonlinear equations resulting from finite element discretization and functional minimization is described. Their solution by efficient computational methods is discussed. These include the Newton-Raphson algorithm, variants of the Gaussian elimination method, and the pre-conditioned conjugate gradient equation solver. Post-processing of the field solution results, in terms of flux plots and parameters such as flux densities, voltages and currents etc., are illustrated.

The chapter presents several applications of the analyses described above to a variety of engineering design problems. These range from no-load and load analyses of utility generators [7, 8], skin effect in busbars [9], eddy-current losses in transformers [10], no-load and starting performance in induction machines [11], dc machine fields [12], permanent magnet device performance prediction [13], eddy-current nondestructive evaluation [14], and electrostatic field applications [15] and others. Comparison of finite-element analysis results with test values

where available are also presented.

a. Two-Dimensional Non-linear Magnetostatic Field

Vector Poisson's Equation and the Functional

In a number of electrical machinery applications, modeling of the geometry of the two-dimensional cross-section is found adequate for design studies. Admittedly this representation neglects end-effects and induced currents in metallic parts. Emphasis is placed exclusively on magnetic saturation of the iron members. Nevertheless, after validation and calibration by tests, the 2D model in many instances has been found to be a useful design tool contributing to engineering productivity and for minimizing prototyping and extensive production testing.

With the foregoing assumptions of time-invariance of the field quantities and of a single valued B-H characteristic, the magnetic field problem may be formulated in terms of the nonlinear Poisson's equation

$$\text{Curl}\,\nu\text{Curl}\,\mathbf{A} = \mathbf{J} \tag{1}$$

where:

ν : reciprocal permeability which is position and field dependent

$\mathbf{A}$: vector potential function with only a 'z' directed component

$\mathbf{J}$: source current density also 'z' directed

Expressing the partial differential (1) in terms of a variational expression called a functional, one obtains as shown in Appendix I

$$F = \int_{\mathrm{v}} \left[\int_0^B \nu\mathbf{B} \cdot d\mathbf{B} - \overline{\mathbf{J}} \cdot \overline{A} \right] d\mathrm{v} - \oint_{\Gamma} \nu\mathbf{A} \frac{\partial A}{\partial n}\, d\Gamma \tag{2}$$

where

$\mathbf{B}$: flux density

n : unit normal to the bounding surface

An approximation to the field solution is sought which makes the functional in (2) stationary, a condition both necessary and sufficient to obtain the correct solution in a least squared sense. Homogeneous boundary conditions of the Dirichlet or Neumann type are satisfied

by setting the line integral in (2) to zero (see Appendix I). This is one of the principal advantages of the finite-element method, wherein no special prescription for imposing natural boundary conditions is necessary. Examination of (2) reveals that it has the dimensionality of energy.

An alternate approach to solving the partial differential (1) which yields the same result as functional minimization is the so-called weighted residual method or the Galerkin method. In this approach, the residual vector of (1) is weighted by a polynomial basis function and integrated over the field region. The resulting expression is transformed by Green's theorem into a volume integral and a surface integral in the same manner as for the functional.

b. Finite-Element Representation

The finite-element procedure consists of subdividing the field region into a discrete number of subregions or elements, and prescribing an approximate solution in each of the subdivisions. This approximation is obtained as a linear combination of solution values at a set of nodes, usually the vertices and interior points weighted by interpolatory functions. The geometrical shape of the element and the approximate solution defined in it describe the finite element. A variety of element shapes are available ranging from the simple planar triangular or quadrilateral elements to the more sophisticated curvilinear isoparametric elements of the first and high order interpolation. In a majority of cases, only function continuity at the nodes and edges of the elements is required.

Figure 5.1 shows first-order triangular and quadrilateral elements which are used in discretizing the field region. The potential solution is defined in terms of the interpolatory functions of the triangular or quadrilateral geometry and the nodal values of potential.

Thus,

$$\mathbf{A} = \sum_{k=i}^{m} \lambda_k A_k \tag{3}$$

where:

λ_k : weighting or shape function

A_k : potential at the kth node

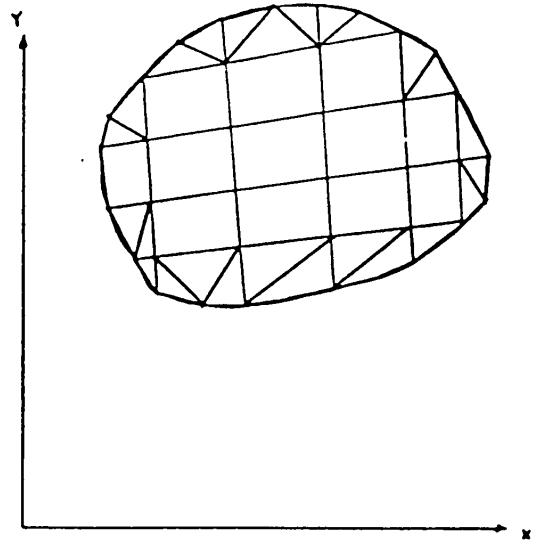

Figure 5.1 Discretization of the field region into triangular and quadrilateral elements.

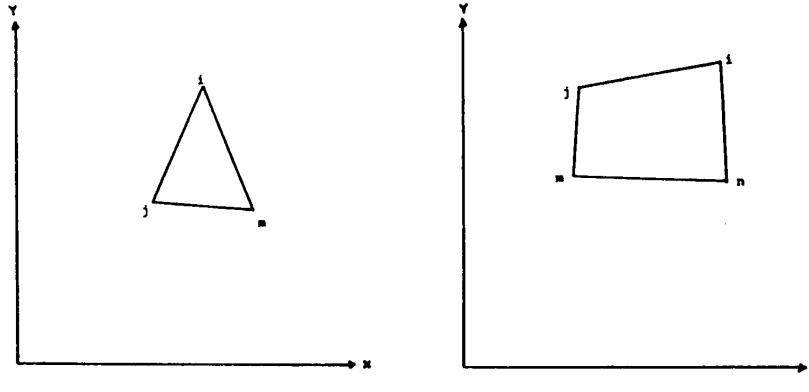

Figure 5.2 First-order elements and weighting functions.

Triangular Element (First Order)

$$\lambda_k = \frac{(a_k + b_k x + c_k y)}{2.\Delta} \qquad k = i, j, m \tag{4}$$

Δ = triangle area

$a_i = x_j y_m - x_m y_j$

$b_i = y_j - y_m$

$c_i = x_m - x_j$

i, j, m in cyclic modulo 3

Quadrilateral Elements (First Order)

$$\lambda_k = \frac{(1 + p\xi)(1 + q\eta)}{4} \qquad \xi = x/a; \quad \eta = y/b \tag{5}$$

a, b are half sides

$p = 1$ for nodes i, n

$= -1$ for nodes j, m

$q = 1$ for nodes i, j

$= -1$ for nodes m, n

The interpolation functions should satisfy the following requirements: (a) that the function corresponding to a node has a unit value at the node and has a zero value when evaluated at the other nodes, (b) their sum must always equal unity. The solution surfaces for typical first order elements are shown in Fig. 5.3.

c. *Magnetic Field Solution*

The solution to the field problem is obtained by either minimizing the functional or by the weighted residual method. In the former, the stationary value of the functional is found by setting its first derivative to zero with respect to each of the values of the approximate potential at each node. For a quadratic functional of the form of (2), the stationary value of the functional is also its minimum value. This procedure

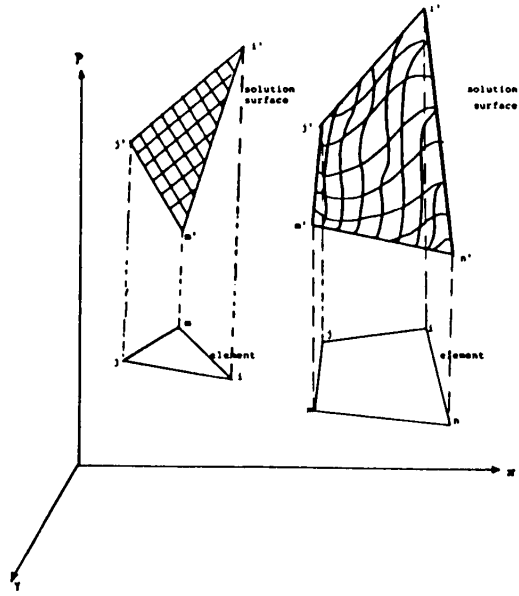

Figure 5.3 Solution surface for first-order elements.

may be formally stated as

$$\frac{\partial F}{\partial A_k}|_{k=1,2,n} = 0 \tag{6}$$

The minimization is carried out over all the finite elements of the field region and the respective matrices are assembled to form a global matrix equation, the solution of which yields the unknown potential A. the matrix equation may be formally stated as

$$[S][A] = [T] \tag{7}$$

In the weighted residual procedure, one applies the Galerkin criterion to the differential Eq. (1) in terms of the interpolation functions $\lambda_i, \lambda_j, \ldots \lambda_n$ and the expansion for **A** is given by Eq. (3) such that

$$\int_v \left[\lambda_i \cdot \text{ curl } \nu \text{ curl } \sum \lambda_k A_k\right] dV - \int_v \lambda_i \cdot J dV = 0 \tag{8}$$

It can be shown that the successive expansion of Eq. (8) over each of the nodes $i, j, m \ldots n$ of the finite element yields the same matrix equation as that obtained by functional minimization in Eq. (6). In the following sections, therefore, further reference to the weighted residual method will not be made.

d. Nonlinear Equations and Iterative Solution.

Equation (7) is nonlinear and matrix $[S]$ is symmetric, sparse and band structured. This equation represents the discretized version of the differential Eq. (1), obtained by a variational procedure. It is quasi-linearized by a quadratically convergent Newton-Raphson algorithm and the resulting set of linear equations is solved directly or iteratively. The reluctivity (reciprocal permeability) is updated in each iteration with respect to the B-H characteristic of the material. The N-R algorithm and the solution of the linear equations are described in Ref.[5] as follows.

Value of the vector potential at the $(k+1)$st iteration is obtained from the value at the kth iteration by the application of the recursive relation

$$A^{k+1} = A^k - [J]^{-1}[SA^k - T] \tag{9}$$

where $[J]$ is the Jacobian matrix of partial derivatives of the iteration function $[SA^k - T]$.

In Ref.[16], the N-R algorithm was directly applied to the functional formulation instead of the residual vector, such that

$$A^{k+1} = A^k - \left[\frac{\partial^2 F}{\partial A_i \cdot \partial A_j}\right]^{-1} \left[\frac{\partial F}{\partial A_i}\right] \tag{10}$$

The above formulation has the attractive feature of providing the theoretical formulation for high order elements.

The set of linearized equations resulting from Eq. (9) is solved by Gaussian elimination technique with node-renumbering [17], profile storage [18], and wave-front solution methods [19]. Recently, however, the pre-conditioned conjugate gradient method has been successfully applied [20] with utmost storage economy and fast execution time.

e. Application to Electrical Apparatus

(i) Two-dimensional vector potential analysis (x-y) in device cross-section

An application of the finite-element method to a single-phase transformer on no-load was described in Ref. [5]. A quarter section of a single-phase inductor was considered with nonlinear magnetic characteristics for the iron core. The analysis was carried out with first-order elements.

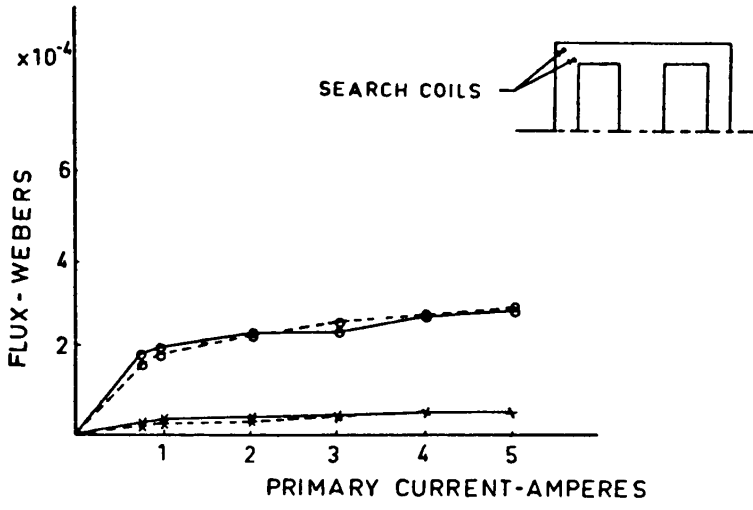

Figure 5.4 Variation of peak flux in the inductor with coil current.

The results of the analysis were compared with search coil test data, as shown in Fig. 5.4. The flux distribution for this case is illustrated in Fig. 5.5.

Application of the nonlinear magnetostatic analysis to a 50 MVA turbine- generator is described by Minnich et al. [8]. The magnetic flux distribution for the no-load condition is illustrated in Fig. 5.6(a). A comparison of test values of open-circuit voltage with finite-element results is shown in Fig. 5.6(b).

During load operation of a rotating electric machine, the axes of symmetry of the magnetic field depart a good deal from the polar and interpolar axes. Under these conditions, the vector potential at any point along the pole axis equals the magnitude at the corresponding point a pole pitch away, but is of opposite sign to the former. This is commonly known as the periodicity condition which can be viewed as an additional boundary condition. Thus the coefficient matrix and forcing function of Eq. (7) are modified such that the sign of the off-diagonal terms corresponding to the points where the periodicity condition applies is reversed. This process is implemented by means of a connection matrix described in Ref.[21]. Figure 5.7 illustrates the shift in the magnetic axis on load for a dc generator shown in Ref.[12].

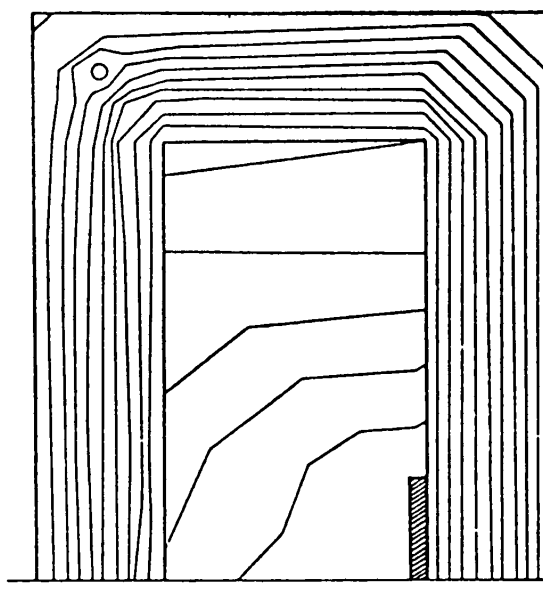

Figure 5.5 Predicted flux distribution in the inductor.

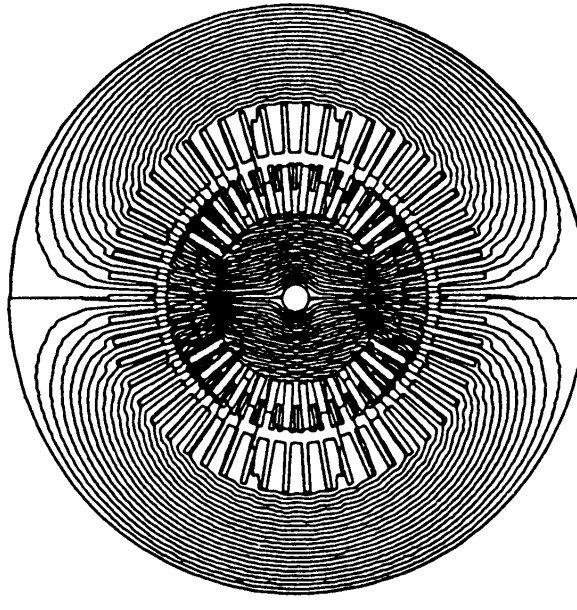

Figure 5.6a Flux distribution in the 50 MVA generator cross-section on no-load.

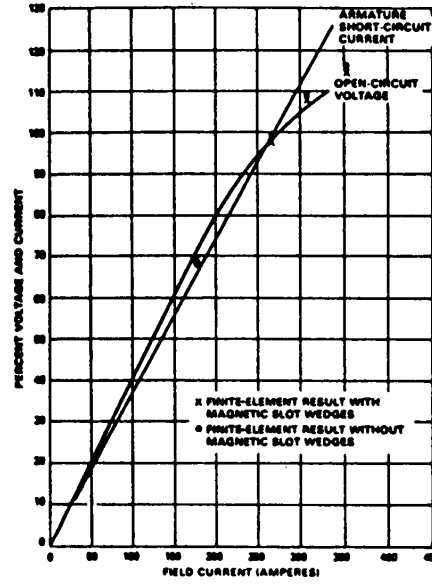

Figure 5.6b Comparison of measured open-circuit voltage with computed values.

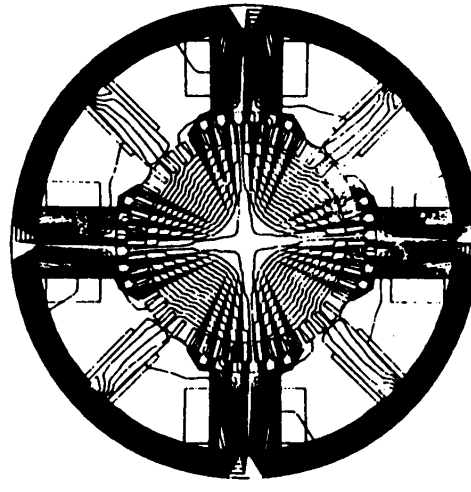

Figure 5.7 Magnetic flux distribution in a dc generator on load.

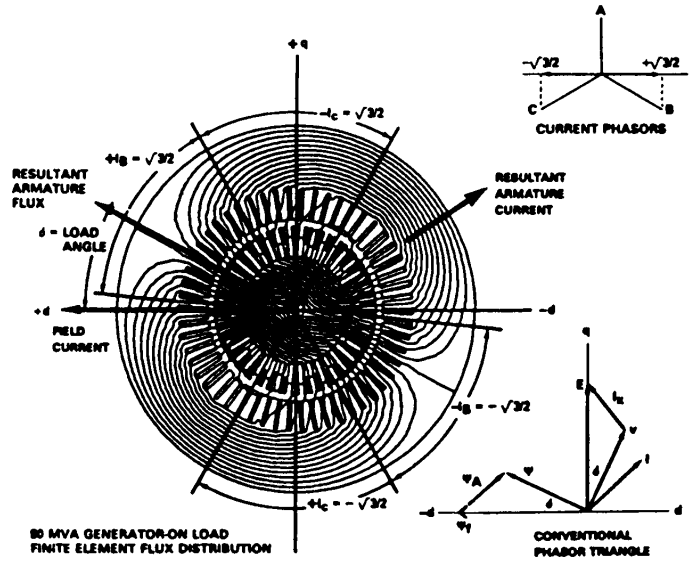

Figure 5.8 Flux distribution in the 50 MVA generator cross section on load.

Minnich et al.[8] applied the finite-element method for analyzing the field distribution in a turbine-generator on steady-state operation for various power factors. A typical flux plot obtained for a loaded generator is shown in Fig. 5.8

Since the time variation of flux is sinusoidal, the induced voltage relates linearly to flux linkages and, hence, also to the vector potential. The flux-linkages in the direct and quadrature axis are calculated in terms of the vector potential which should accurately yield the direct and quadrature components of voltage. In general, this is a two-step process. Brandl, Reichert, and Vogt[22] suggested an alternative scheme employing the N-R technique. In this method, the constraint conditions on the terminal quantities are imposed explicitly.

(ii) Axiperiodic Scalar Potential Analysis

In special applications of electrical machinery, one needs to determine end-leakage effects such as end-leakage reactances, and forces on windings. Whereas a full-fledged three-dimensional analysis is desirable, a more economical solution such as by axiperiodic analysis may suffice. In this section we shall illustrate a scalar potential axiperi-

odic formulation and its application to the end-region of a turbine-generator.

The partial differential equation which governs the field distribution in the axisymmetric geometry of the device with an axiperiodic excitation is given by Eq. (11a).

$$\nabla \cdot \mathbf{B} = \nabla \cdot \mu \mathbf{H} = -\nabla \cdot \mu \nabla \phi = 0 \qquad (11a)$$

The corresponding functional formulation is described by Eq. (11b). Minimization of Eq. (11b),

$$\varepsilon = \frac{1}{2} \iiint \left[\mu_{rr} \left(\frac{\partial F}{\partial r} \right)^2 + \mu_{zz} \left(\frac{\partial F}{\partial z} \right)^2 + \frac{n^2 \mu_{\theta\theta}}{r^2} F^2 \right] dV \qquad (11b)$$

yields a set of matrix equations, which when solved by an N-R procedure yields the required potential solution. The gradient of the scalar potential yields the magnetic field distribution. At discontinuities such as the excitation current source, a jump in the magnetic field is essential with the scalar potential formulation.

Traditional methods of imposing branch-cuts are cumbersome and complicated. A new development known as a "gap-element" adequately models the jump discontinuity in the magnetic field at the air-conductor interface. The excitation source is decomposed into a set of harmonics, each of which requires a separate finite element solution. These solutions summed over all the harmonics yield the desired result.

The above method is described in detail in Ref.[23], wherein its application to the end-region of a turbine generator is illustrated. Figure 5.9 shows the scalar potential distribution in the generator cross-section.

5.2 Modeling of Permanent Magnet Devices

In the magnetic field analysis presented in this section, the following assumptions are made in deriving the associated partial differential equation:

- The magnetic field is time invariant and stationary.
- The source function is represented by a constant current density distribution in ideal conductors carrying current. In the case of the

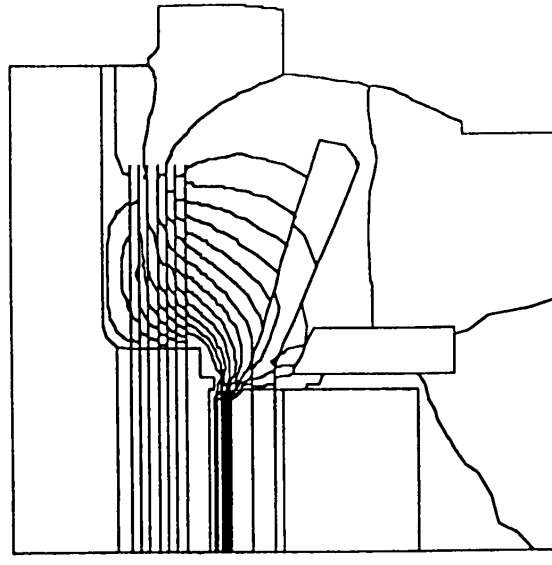

Figure 5.9 Equipotential Contours.

permanent magnets, the source function is represented either by current sheets or moment distribution.

- The permeability is isotropic and either a constant or a function of the vector potential. The B-H curves are assumed to be single valued and hysteresis is neglected.
- In the case of samarium cobalt magnets and ferrites, the magnetic moment is assumed to be unidirectional and uniform over the pole cross section. In the case of Alnico magnets, the moment distribution is considered non-uniform, having more than one component.
- A vector potential formulation is employed for two-dimensional fields and a scalar potential formulation is employed for three-dimensional problems.

Subject to the above assumptions, the following Maxwell's equations hold.

The flux-density $\mathbf{B}$, the magnetizing force $\mathbf{H}$, and the intrinsic magnetization $\mathbf{M}$ of a permanent magnet material are related by

$$\mathbf{B} = \mu_o(\mathbf{H} + \mathbf{M}) \tag{12}$$

It is convenient to represent the intrinsic magnetization by

$$\mathbf{M} = \chi\mathbf{H} + \mathbf{M}_o \tag{13}$$

where $\mathbf{M}_o$ is the remanent intrinsic magnetization of constant magnitude in the anisotropic direction and χ is the susceptibility, which is a function of $\mathbf{H}$ in a nonlinear material. By combining Eqs. (12) and (13) and using the nomenclature $\mu_r = 1 + \chi$, we have,

$$\frac{\mathbf{B}}{\mu_o} = \mu_r \mathbf{H} + \mathbf{M}_o \tag{14}$$

Re-writing (14) yields

$$\mathbf{H} = \nu \mathbf{B} - \frac{\nu}{\nu_o} \mathbf{M}_o \tag{15}$$

where ν is the reciprocal permeability equal to $\frac{1}{\mu_r \mu_o}$ and ν_o is the reluctivity of free space which equals $\frac{1}{\mu_o}$

a. Vector Potential Formulation

We may choose a vector potential function defined as

$$\mathbf{B} = \text{Curl}\, \mathbf{A} \tag{16}$$

Substituting for $\mathbf{B}$, in Eq. (15) for the value given in (16)

$$\mathbf{H} = \nu \text{Curl}\, \mathbf{A} - \frac{\nu}{\nu_o} \mathbf{M}_o \tag{17}$$

If there are discrete source currents present, then Ampere's law holds. Thus,

$$\text{Curl}\, \mathbf{H} = \text{Curl}\, \nu \text{Curl}\, \mathbf{A} - \text{Curl}\, \frac{\nu}{\nu_o} \mathbf{M}_o = \mathbf{J}_s \tag{18}$$

where $\mathbf{J}_s$ is the source current density.

Equation (18) represents the vector Poisson equation for the permanent magnet machine or device which can be specialized to the different regions as follows:

- Source free region

$$\nu_o \text{Curl}\, \text{Curl}\, \mathbf{A} = 0 \tag{19}$$

- Source free region external to the magnet

$$\text{Curl}\, \nu(\mathbf{A}) \text{Curl}\, \mathbf{A} = 0 \tag{20}$$

- Magnet region

$$\text{Curl}\,\nu(\text{A})\text{Curl}\,\text{A} - \text{Curl}\,\frac{\nu}{\nu_o}(\text{A})\text{M}_o = 0 \tag{21}$$

- Source region external to the magnet

$$\nu_o \text{Curl}\,\text{Curl}\,\text{A} = \text{J}_s \tag{22}$$

For a set of partial differential equations represented by

$$DA = \psi \tag{23}$$

where D is a symmetric operator, the variational formulation is defined by the functional

$$F = \langle A^T | DA \rangle - 2\langle A^T | \psi \rangle \tag{24}$$

where the inner product <> represents the integration and superscript T denotes transposition. Substituting the curl curl operator of (18) for D and then performing the indicated operations of (24), one obtains the expression for the energy related functional as

$$F = \iint_s \left[\text{A} \times (\text{H} + \text{H}') \cdot \text{ds} + \int_\Omega \int_o^B \nu \left(\text{B} - \frac{\text{M}_o}{\nu_o}\right) \cdot \text{dB}\right] d\Omega - \int_\Omega (\text{A} \cdot \text{J}_s)\, d\Omega \tag{25}$$

It can be shown that after setting the surface integral of (25) to zero, the Euler equation associated with the functional, i.e., the integrand of the volume integral in (25), yields the curl curl Eq.(18).

According to the calculus of variations [24], the vector function A, which extremizes the above functional, is a solution of the associated differential Eq. (18) subject to the natural boundary conditions obtained when setting the surface integral in the functional expression of (25) to zero.

b. Two Dimensional Fields

(i) Field Problem in Cartesian Coordinates. The functional minimization process described above yields a matrix equation for the two-dimensional problem in Cartesian coordinates, as

$$\left.\frac{\partial F}{\partial A_k}\right|_{k=i,j,m} = \left[\nu \sum_{1=i,j,M} S_{k1} A_1 + \frac{\nu}{2\nu_o}(M_{oy} b_k - M_{ox} c_k) - \frac{J_s \Delta}{3}\right] |_{k=i,j,m} = 0 \quad (26)$$

where Δ is the triangle area,

$$S_{k1} = \frac{b_k b_1 + c_k c_1}{4\Delta}$$
$$b_k = y_j - y_m \text{ and}$$
$$c_k = x_m - x_j$$

In matrix notation Eq. (26) becomes

$$\nu \begin{bmatrix} S_{ii} & S_{ij} & S_{im} \\ & S_{jj} & S_{jm} \\ sym & & S_{mm} \end{bmatrix} \begin{bmatrix} A_i \\ A_j \\ A_m \end{bmatrix} = \frac{\nu}{\nu_o}\frac{M_{ox}}{2} \begin{bmatrix} C_i \\ C_j \\ C_m \end{bmatrix} - \frac{\nu}{\nu_o}\frac{M_{oy}}{2} \begin{bmatrix} b_i \\ b_j \\ b_m \end{bmatrix} + \frac{J|\Delta|}{3} \begin{bmatrix} 1 \\ 1 \\ 1 \end{bmatrix} \quad (27)$$

Equation (27) represents the general two-dimensional representation of the permanent magnet device in Cartesian coordinates. The magnet moment is expressed with both its components in the xy-plane and, therefore, is of general application to a wide variety of permanent magnet materials.

The advantage of this formulation is that, even if the magnet has a complex profile, the user does not have to calculate equivalent currents or make special efforts at modeling.

If however, the magnet is uniformly magnetized, representation of the field problem by Eq. (27) will be identically the same as modeling by equivalent current sheets.

(ii) Axisymmetric Problem. Substituting for **B** the value equals $\{\frac{\partial A}{\partial z}\hat{r} - \frac{\partial}{\partial r}\left(r\frac{\partial A}{\partial r}\right)\hat{z}\}$ in (25) and implementing (27) after setting the surface integral to zero, one obtains the expression

$$\frac{\partial F}{\partial \phi_k}|_{k=i,j,m} = 0 = 8\pi\Delta \iint \left\{\nu\left[r_o^2\left(\frac{\partial \zeta_i}{\partial r}\right)\left(\frac{\partial \zeta_j}{\partial r}\right) + \frac{3r_o}{2}\left[\zeta_i\frac{\partial \zeta_j}{\partial r} + \zeta_j\frac{\partial \zeta_i}{\partial r}\right]\right.\right.$$
$$\left.\left. + \frac{9}{4}\zeta_i\zeta_j + r_o^2\left(\frac{\partial \zeta_i}{\partial r}\right)\left(\frac{\partial \zeta_j}{\partial r}\right)\right]\phi_i - r_o^2\zeta_i\zeta_j\psi_i\right\} dr\,dz \tag{28}$$

where $\mathbf{A} = \sqrt{r}\phi$ and $M = \sqrt{r}\psi$

When the minimization (26) and (28) are carried out over all triangles and the individual terms are evaluated, the following set of equations is obtained.

$$[S][A] = [R] \tag{29}$$

c. Applications

The two-dimensional magnetostatic Finite Element analysis was applied to a radial permanent magnet motor of novel design [25], a magneto-fluidic seal of axisymmetric geometry and an illustrative example of a magnetic clutch.

(i) Radial PM Motor. The outline, finite element triangulation, and the flux plots for the no-load and load conditions for a radial two-pole permanent magnet machine are shown in Figs. 5.10 through 5.13.

(ii) Magnetic Fluid Seal. The axisymmetric finite element field analysis was applied to a positive pressure gas-to-gas magnetic fluid seal [26] for large-diameter high-speed shaft applications. The objective is to determine the effectiveness of the seal by computing the radial and tangential forces from the magnetic field distribution. The seal is designed to operate in a 10-inch diameter shaft, at peripheral speeds of 4000 fpm or more, to withstand pressure up to 7 psig, to operate under large circumferential variations of the stator-rotor gap (from 0.03 to 0.01 inch), and with background axisymmetric magnetic fields of flux-densities up to 0.5T.

The cross section of the magnetic fluid seal, the two-dimensional model outline, the flux-distribution obtained without the background field, and the plot of the radial flux density variation along the rotor-stator gap are illustrated in Figs. 5.14, 5.15, 5.16, and 5.17, respectively.

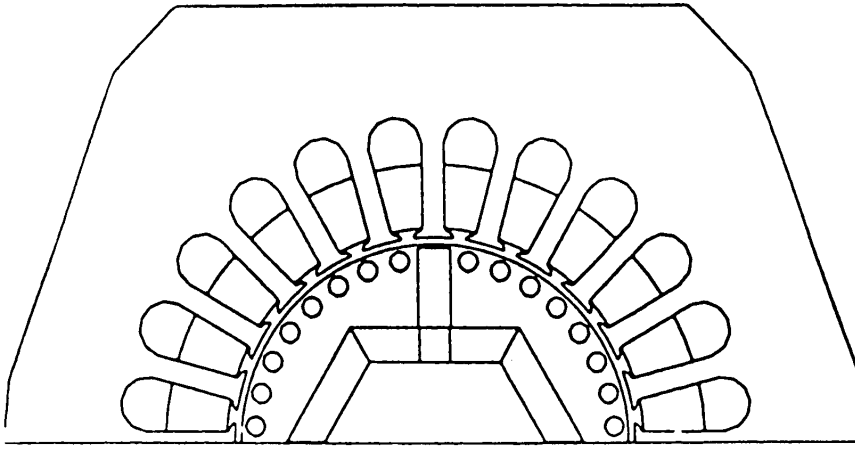

Figure 5.10 Outline of the two-pole motor.

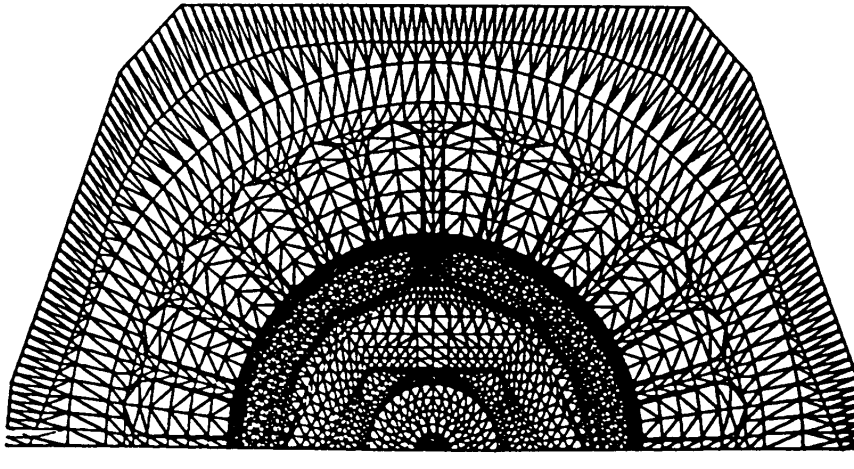

Figure 5.11 Finite Element Triangulation of PM motor cross section.

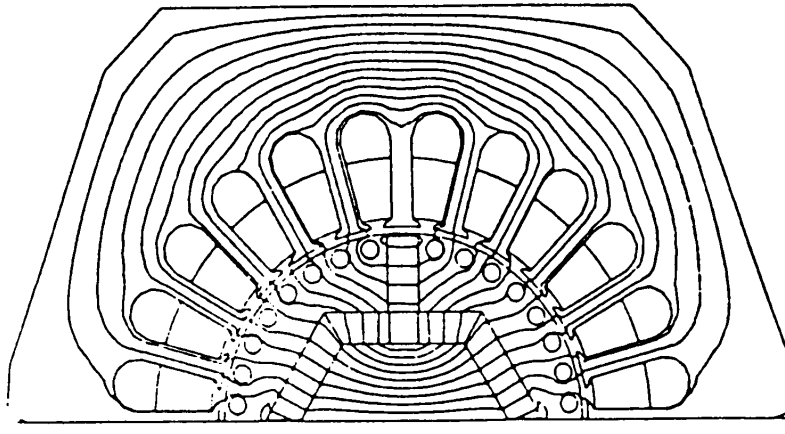

Figure 5.12 Flux-Distribution on no-load for the PM motor.

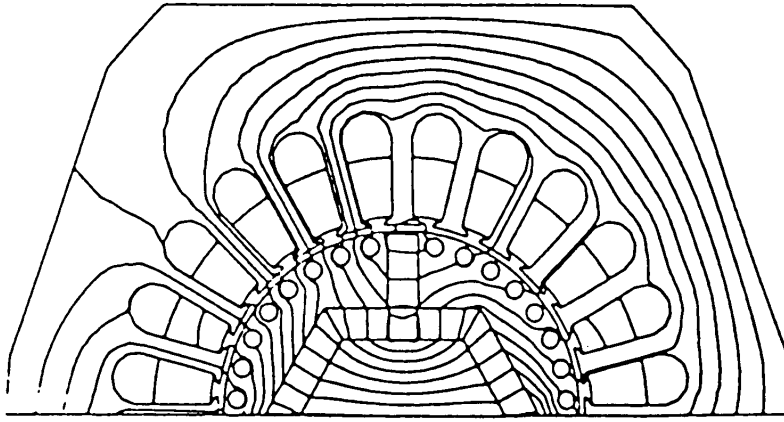

Figure 5.13 Flux-Distribution in the PM motor on load.

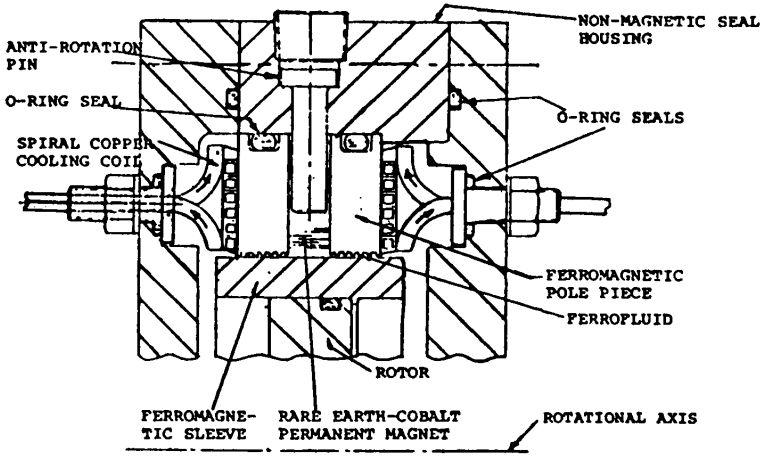

Figure 5.14 Cross section of magnetic fluid seal.

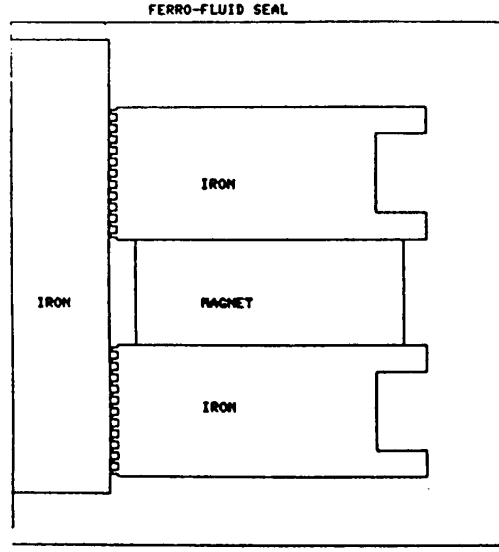

Figure 5.15 Axisymmetric model outline of the seal.

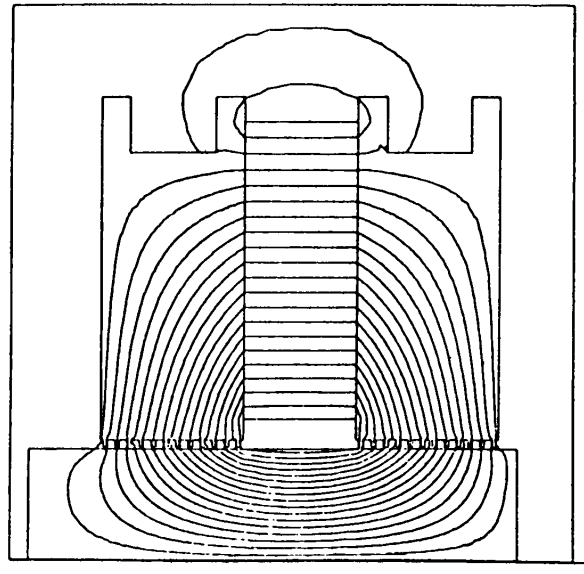

Figure 5.16 Flux-Distribution in magnetic fluid seal.

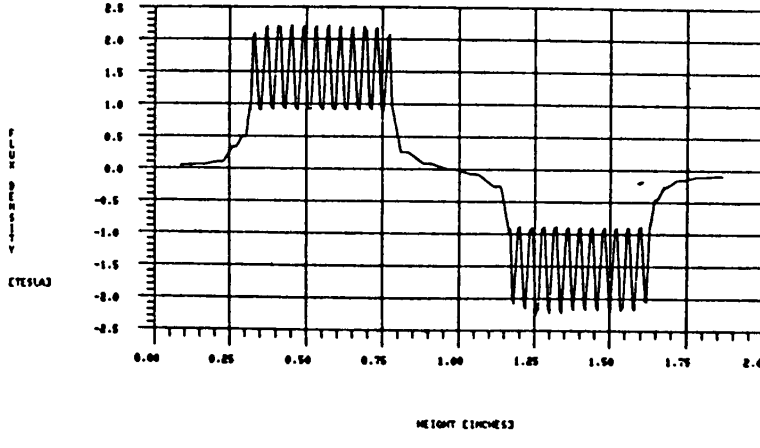

Figure 5.17 Radial flux-density in rotor-stator gap of magnetic fluid seal

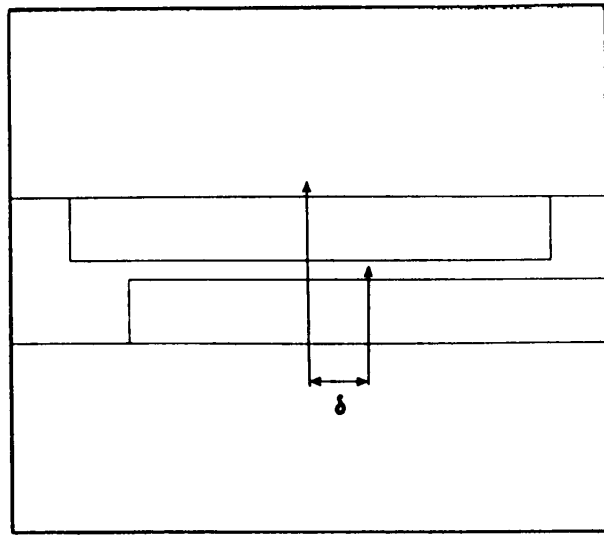

Figure 5.18 Two-Dimensional cross section of a portion of a magnetic clutch.

(iii) Magnetic Clutch. The principle of the Rotating Magnetic Clutch is illustrated with respect to the developed view of the two-dimensional cross section of a portion of the clutch, shown in Fig. 5.18. The objective of this analysis is to determine the shear force variation with the clutch angle that was measured from the axis of the clutch. This section describes the flux-distribution obtained for several angular positions of the moving parts of the clutch, the method of computing the shear force by the Maxwell's stress tensor, and the results obtained.

The flux-distributions obtained for several angular positions for the permanent magnet rotating clutch are shown in Figs. 5.19 through 5.22.

d. Forces on the Permanent Magnet Clutch

The tangential and normal forces on the magnetic clutch are obtained by integrating the Maxwell stress tensor over the respective surfaces.

The stress tensor is given by diadic [27]

$$F = \nabla \left(BB - 1/2IB^2 \right) \tag{30}$$

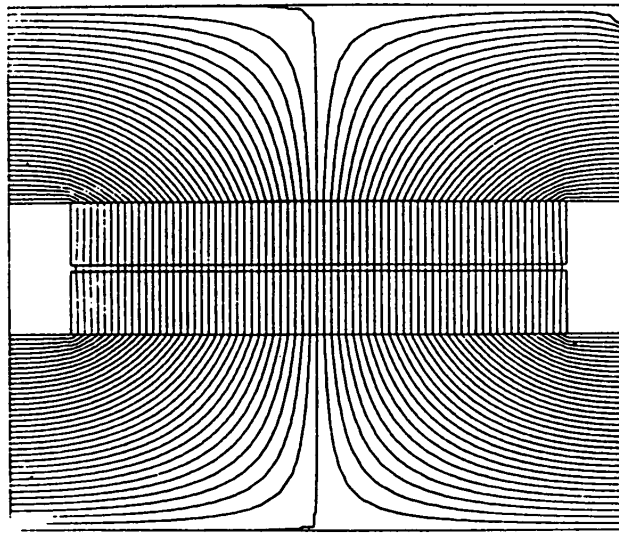

Figure 5.19 Flux-Distribution in magnetic clutch; $\delta = 0°$.

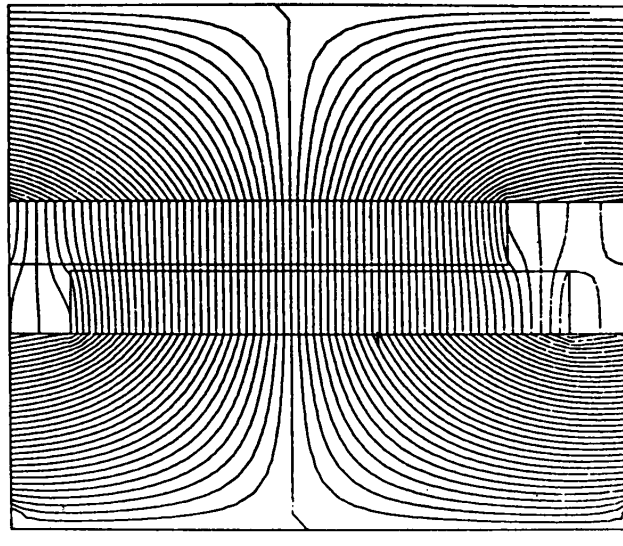

Figure 5.20 Flux-Distribution in magnetic clutch; $\delta = 18°$.

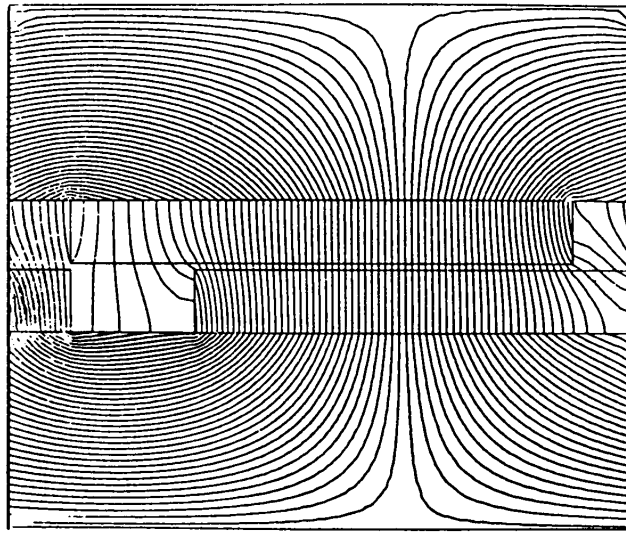

Figure 5.21 Flux-Distribution in magnetic clutch; $\delta = 36°$.

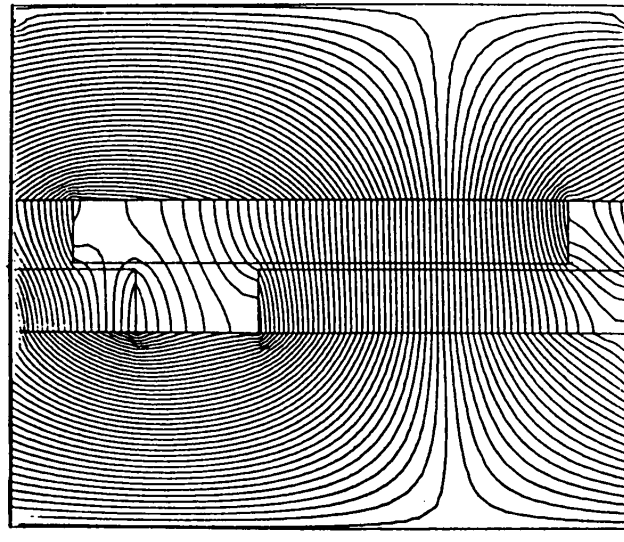

Figure 5.22 Flux-Distribution in magnetic clutch; $\delta = 54°$.

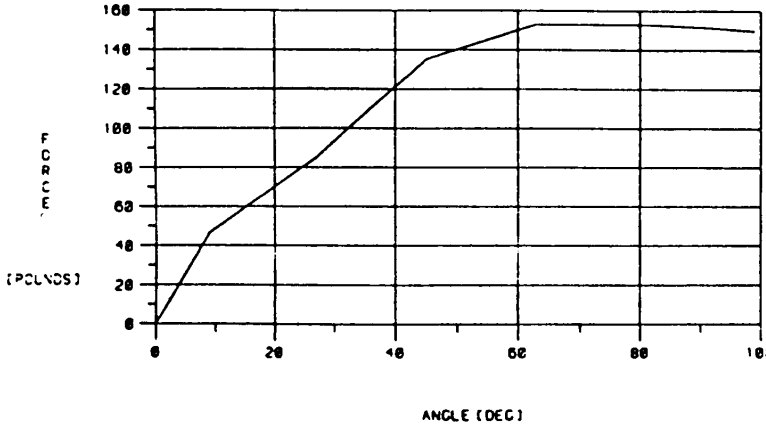

Figure 5.23 Shear force distribution in the magnetic clutch.

The shear force f_s on the magnetic clutch is given by

$$f_s = \int \mu_r \mu_s H_x H_y dx dy \tag{31}$$

Where H_x and H_y are the components of the magnetizing force.

The shear force variation with the clutch angle is shown in Fig. 5.23.

5.3 Analysis of the Eddy-Current Diffusion Problem

a. Two-dimensional Fields

The first application of the eddy-current diffusion analysis by finite elements, for geophysical prospecting, was described by Silvester and Haslam [28]. A similar formulation was presented in Ref.[29] for linear eddy-current problems in magnetic structures. The governing differential equation and functional for two-dimensional problems are given as follows. The functional is derived in Appendix II.

$$\nu \text{div}(\text{grad } \mathbf{A}) = j\omega\sigma\mathbf{A} - \mathbf{J}_s \tag{32}$$

$$F = \iint \left[\nu(\text{grad } \mathbf{A})^2 + j\omega\sigma\overline{\mathbf{A}} \cdot \overline{\mathbf{A}} - 2\overline{\mathbf{J}}_s \cdot \overline{\mathbf{A}}\right] dx dy \tag{33}$$

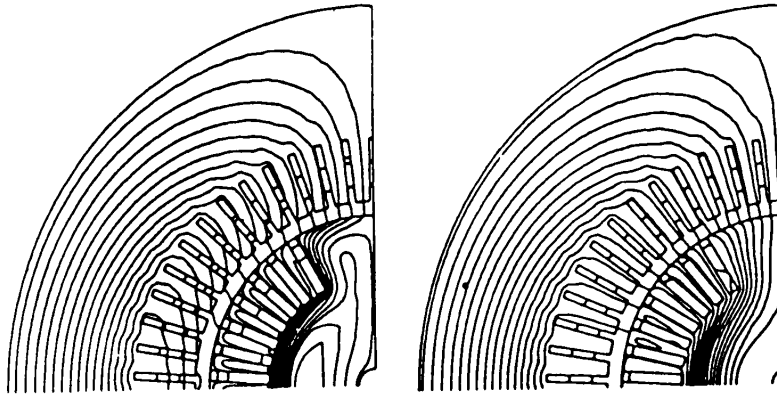

Figure 5.24 Flux plots for 0.1 Hz d-axis current. Left: real component; right: imaginary component.

The minimization of the functional in Eq. (33) leads to a complex matrix equation

$$[S][A] + [C][A] = [T] \tag{34}$$

The above analysis was applied to semi-infinite and finite width conducting slabs and the results were compared with test values, with good agreement, as shown in Ref. [29].

Another application of the method to a utility generator for obtaining operational impedances was described in Ref. [30]. The flux plots obtained at 0.1 Hz are shown in Fig. 5.24. The steady-state diffusion equation solution was also applied to the nondestructive evaluation of a crack in a rod of aluminum as illustrated in Figs. 25(a) and (b). Donea, Giuliani, and Philippe [31] presented the analysis of an electromagnetic induction heating problem in axisymmetric geometry with a "θ" directed vector potential $A_\theta(r, z)$.

Foggia et al. [32] described the solution of the saturated magnetic field problem in a linear induction motor. The partial differential equation was modified to include a velocity term V so that

$$\frac{\partial}{\partial x}\left(\frac{1}{\mu}\frac{\partial A}{\partial x}\right) + \frac{\partial}{\partial y}\left(\frac{1}{\mu}\frac{\partial A}{\partial y}\right) = \sigma\frac{\partial A}{\partial t} + V\frac{\partial A}{\partial x} \tag{35}$$

An alternative to the functional minimization process was presented

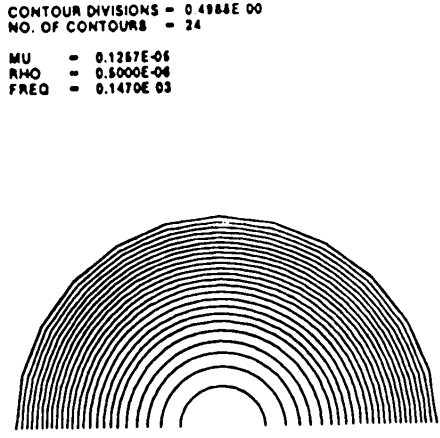

Figure 5.25a Real part of eddy-current profile in cross section of round bar without crack.

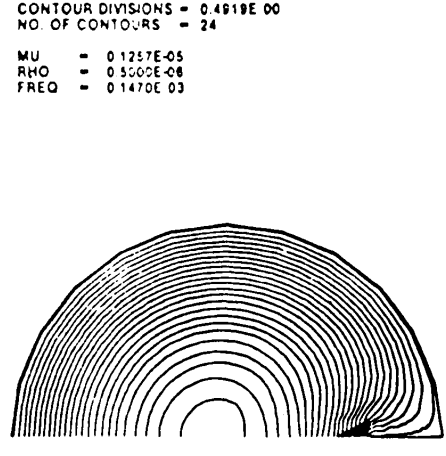

Figure 5.25b Real part of eddy-current profile in cross section of round bar with crack.

using the weak Galerkin formulation with the result

$$\int_\Omega \left(\frac{\partial A}{\partial t} + V\frac{\partial A}{\partial x}\right)\phi(x,y)dxdy + \int_\Omega \rho\nu\left(\frac{\partial A}{\partial x}\frac{\partial V}{\partial x} + \frac{\partial A}{\partial y}\frac{\partial V}{\partial y}\right)dxdy = 0 \tag{36}$$

where ϕ is required to vanish whenever essential boundary conditions apply to A on the boundary. Substituting the finite-element approxi-

mation of **A** in Eq. (36), yields the time-dependent matrix equation

$$[M]\frac{d}{dt}[A] + [N][A] = 0 \tag{37}$$

which was solved by a time-stepping technique.

Csendes and Chari [33] described a general variational formulation for the diffusion problem, including the rotational terms. This generalization of the eddy-current problem is suited for analyzing the asynchronous performance of rotating electrical machines.

In this method, the partial differential equation and its functional formulation are given by

$$\nu \operatorname{div}(\operatorname{grad}\mathbf{A}) = \sigma\left(\frac{\partial \mathbf{A}}{\partial t} + V \times \mathbf{B}\right) - \mathbf{J}_s \tag{38}$$

$$F = \int_R (\operatorname{grad}\mathbf{A})^2 dR + \sigma\mu\omega \int_R \left(y\frac{\partial \mathbf{A}}{\partial x} - x\frac{\partial \mathbf{A}}{\partial y}\right) dR + j\sigma\mu\omega \int_R \mathbf{A}^2 dR - 2\int_R \mathbf{A}\cdot\mathbf{J}_s dR \tag{39}$$

The above technique was applied to a simplified generator cross section discretized by first order triangular elements.

b. Skin Effect by Integro-differential Method

Konrad and Chari [9] described the skin-effect problem by an integrodifferential formulation of the form

$$\nu \operatorname{div}(\operatorname{grad}\mathbf{A}) - j\omega\sigma\mathbf{A} = -\frac{I + j\omega\sigma \iint \mathbf{A}\cdot ds}{\iint ds} \tag{40}$$

The corresponding functional is given by

$$F = \int_v \left[(\operatorname{grad}\mathbf{A})^2 + j\omega\sigma\mathbf{A}^2 - j\omega\sigma\mathbf{A}\cdot\frac{\Sigma\Sigma\mathbf{A}ds}{\Sigma\Sigma ds}\right] dv - \int_v 2\mathbf{J}\cdot\mathbf{A}dV \tag{41}$$

The solution obtained for a transmission line bundle conductor arrangement is shown in Fig. 5.26.

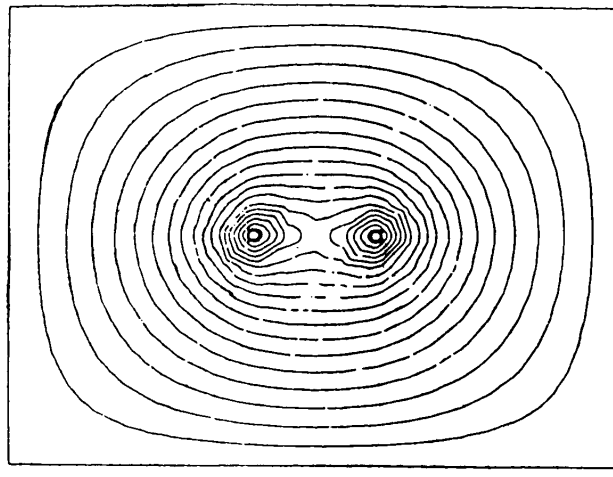

Figure 5.26 Flux distribution in a five-wire bundle conductor arrangement.

c. The Superposition Method

As an alternate to the integro-differential formulation method described in the previous section, one may consider a superposition method.

In the event of having N conductors with N known total currents $I_i (i = 1 \text{ to } N)$, one can arrive at a solution by solving the differential Eq. (32) N times. Each time, a different conductor is assumed to carry a unit current density, in place of $\mathbf{J}_s$ while all other conductors are assumed to carry no net current. Let the vector potential solution so obtained be designated A_j.

The finite element procedure to obtain A_j has already been described, as one of approximating A_j by a linear combination of a complete set of interpolation polynomials defined over a two-dimensional triangular finite element. The operator of Eq. (32) was discretized to yield a symmetric complex matrix equation, which is then solved for A_j.

The solution to the original field problem can be expressed as a linear combination of the different solutions for A_j obtained by inputing unit current density in each of the sheet windings successively.

Thus the total solution is given by

$$\mathbf{A} = \sum_{j=1}^{N} C_j A_j \tag{42}$$

Equation (42) represents a straightforward application of the principle of superposition. It remains only to determine the N constants C_j such that the integral form of condition of Eq. (42) holds for the i-th conductor ($i = 1$ to N), i.e.,

$$I_i = \iint \mathbf{J}_{ti} \cdot d\mathbf{S} = \iint \mathbf{J}_{si} \cdot d\mathbf{S} - j\omega\sigma_i \sum_{j=1}^{N} C_j \iint \mathbf{A}_j \cdot d\mathbf{S} \tag{43}$$

It must be noted that the last integral represents the eddy currents induced in terms of the vector potential solution obtained in Eq. (42). The procedure described by Eq. (43) leads to a system of N equations in N unknowns that can be solved for C_j. The integrations in Eq. (43) are over the conductor cross-section. In matrix form, Eq. (43) may be expanded as follows

$$\begin{bmatrix} J_{s1} \cdot \square_1 \\ J_{s2} \cdot \square_2 \\ \vdots \\ J_{sN} \cdot \square_N \end{bmatrix} - jw \begin{bmatrix} \sigma_1 \sum_{\text{condr1}} \mathbf{A}_1 \cdot \text{ds} \\ \sigma_2 \sum_{\text{condr2}} \mathbf{A}_1 \cdot \text{ds} \\ \vdots \\ \sigma_N \sum_{\text{condrN}} \mathbf{A}_1 \cdot \text{ds} \end{bmatrix}$$

$$\begin{matrix} \sigma_1 \sum_{\text{condr1}} \mathbf{A}_2 \cdot \text{ds} & \cdots & \sigma_1 \sum_{\text{condr1}} \mathbf{A}_N \cdot \text{ds} \\ \sigma_2 \sum_{\text{condr2}} \mathbf{A}_2 \cdot \text{ds} & \cdots & \sigma_2 \sum_{\text{condr2}} \mathbf{A}_N \cdot \text{ds} \\ \\ \sigma_N \sum_{\text{condrN}} \mathbf{A}_2 \cdot \text{ds} & \cdots & \sigma_N \sum_{\text{condrN}} \mathbf{A}_N \cdot \text{ds} \end{matrix} \begin{bmatrix} C_1 \\ C_2 \\ \vdots \\ C_N \end{bmatrix} = \begin{bmatrix} I_1 \\ I_2 \\ \vdots \\ I_N \end{bmatrix} \tag{44}$$

where $\square$ represents the area over the winding; $\mathbf{J}_{s1}, \mathbf{J}_{s2} \ldots$ are source current densities which are input in the superposition analysis, $\sigma_1, \sigma_2 \ldots_N$ are conductivities; $\mathbf{A}_1, \mathbf{A}_2 \ldots$ are the vector potential solutions obtained with successive excitation of the windings. For example,

$\mathbf{A}_1$ refers to the vector potential solution obtained in the first winding due to excitation by the source current density $\mathbf{J}_{s1} \cdot C_1, C_2 \ldots$ are the unknown coefficients; and $I_1, I_2, \ldots I_N$ are the respective currents (total).

Once the C_js are determined, the vector potential solution is obtained from Eq. (42).

d. Axiperiodic Analysis

We calculate the eddy current effects in the end region of a generator using a vector potential formulation for the magnetic induction, **B**:

$$\mathbf{B} = \nabla \times \mathbf{A} \tag{45}$$

It should be noted here that **B** refers only to that part of the magnetic induction which varies with time in the rotor coordinate system. It is assumed to be a perturbation on the DC components. The associated magnetic field, **H**, is related to the magnetic induction by the reluctivity tensor:

$$\begin{bmatrix} H_r \\ H_z \\ H_\theta \end{bmatrix} = \begin{bmatrix} \nu_{rr} & 0 & 0 \\ 0 & \nu_{zz} & 0 \\ 0 & 0 & \nu_{\theta\theta} \end{bmatrix} \begin{bmatrix} B_r \\ B_z \\ B_\theta \end{bmatrix} \tag{46}$$

As in the magnetostatic case, the orthotropic properties model laminations, teeth, and intrinsic material properties. However, here the properties are taken in the incremental sense, i.e., they represent small excursions on the magnetization curve [34].

Using a gauge in which the scalar electric potential is set to zero, the electric field, **E**, is

$$\mathbf{E} = -j\omega\mathbf{A} \tag{47}$$

and the eddy current density (not source current density) is

$$\begin{bmatrix} J_r \\ J_z \\ J_\theta \end{bmatrix} = \begin{bmatrix} \sigma_{rr} & 0 & 0 \\ 0 & \sigma_{zz} & 0 \\ 0 & 0 & \sigma_{\theta\theta} \end{bmatrix} \begin{bmatrix} E_r \\ E_z \\ E_\theta \end{bmatrix} \tag{48}$$

The conductivity tensor, like the reluctivity tensor, models geometric effects (e.g. laminations and teeth) as well as material properties.

Again, we decompose the potential in a Fourier series. Since the solution is complex, we combine the sine and cosine parts in one complex term which represents a rotating field:

$$\mathbf{A} = \sum_{n=1}^{N} e^{jn\theta} F_n(r,z) \tag{49}$$

As before, we deal with each term in (49) separately. Unlike the magnetostatic case, the incremental permeabilities are not functions of the solution, and so iteration is not needed.

The functional for the finite element analysis is [23]

$$\begin{aligned}\varepsilon = \frac{1}{2}\iiint \Bigg[& \frac{\nu_{rr}}{r^2}\left(jnF_z - r\frac{\partial F_\theta}{\partial z}\right)^2 + \nu_\theta\left(\frac{\partial F_r}{\partial z} - \frac{\partial F_z}{\partial r}\right)^2 \\ & + \frac{\nu_{zz}}{r^2}\left(F_\theta + r\frac{\partial F_\theta}{\partial r} - jnF_r\right)^2 \\ & - 2F_r J_r^s + F_z J_z^s + F_\theta J_\theta^s \\ & + \frac{\lambda\nu_0}{r^2}\left(F_r + r\frac{\partial F_r}{\partial r} + r\frac{\partial F_z}{\partial z} + jnF_\theta\right)^2 \Bigg] dV\end{aligned} \tag{50}$$

where $\mathbf{J}^s$ is the source current density, which we assume to be eddy-free. The last term in (50) is a penalty function with an adjustable, dimensionless parameter, λ. It enforces

$$\nabla \cdot \mathbf{F} = 0 \tag{51}$$

which is simply the non-divergence of $\mathbf{E}$ in the absence of volume charges. Equation (51) is valid only within material volumes. At material interfaces, the tangential components of $\mathbf{E}$ and the normal component of $\mathbf{J}$ are continuous.

We use gap elements, which we call in this case "continuity elements," to enforce continuity of the respective fields. As before, two nodes are created at the same physical location. The material interface is rotated at some angle in the (r,z) plane. (see Fig.5.27.)

Continuity of the tangential components of $\mathbf{E}$ is satisfied by

$$\cos(\phi_{ij})F_{j,r} + \sin(\phi_{ij})F_{j,z} = \cos(\phi_{ij})F_{i,r} + \sin(\phi_{ij})F_{i,z} \tag{52}$$

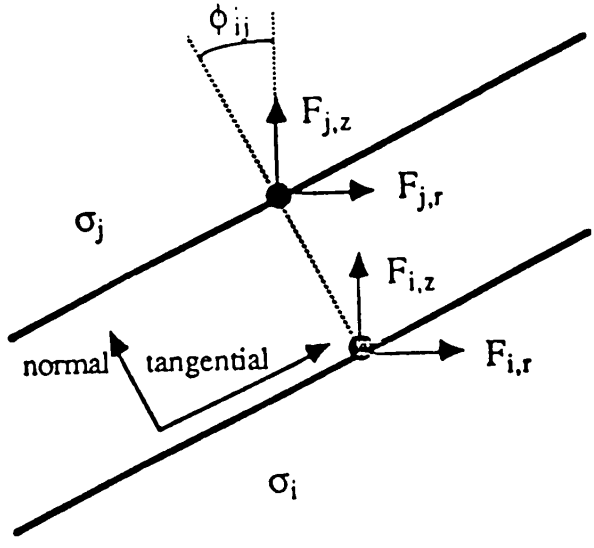

Figure 5.27 Continuity element.

and

$$F_{j,\theta} = F_{i,\theta} \tag{53}$$

while continuity of the normal component of **J** is satisfied by

$$\begin{aligned} &-\sin(\phi_{ij})\sigma_{j,rr}F_{j,r} + \cos(\phi_{ij})\sigma_{j,zz}F_{j,z} = \\ &-\sin(\phi_{ij})\sigma_{i,rr}F_{i,r} + \cos(\phi_{ij})\sigma_{i,zz}F_{i,z} \end{aligned} \tag{54}$$

Using (52) and (53), we eliminate the variables at node j in favor of the variables at node i (assuming the conductivity is greater at node j).

Figure 5.28 shows the eddy distribution as calculated with our software in a metallic object similar to a retaining ring. The lengths of the arrows are proportional to the current density. Where current seems to be diverging near the top of the object, it is actually turning to the peripheral direction, which is out of the plane of the figure. Once the eddy current solution has been calculated, our thermal analysis program can automatically extract the power losses.

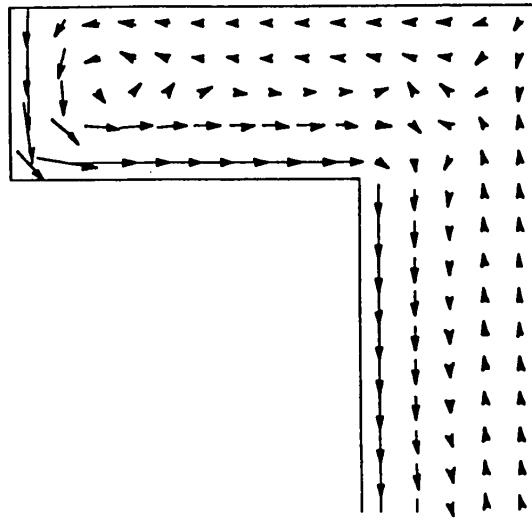

Figure 5.28 Eddy currents near corners.

5.4 Three Dimensional Fields

a. Vector Potential Formulation

The three-dimensional nonlinear magnetostatic field problem obtained by a vector potential function can be formulated by the following partial differential equations derived from Maxwell's equations

$$\text{Curl}\,\nu\text{Curl}\,\mathbf{A} = \mathbf{J} \tag{55}$$

$$\text{div}\mathbf{A} = 0 \tag{56}$$

The functional expression for Eqs.(55) and (56) is given in terms of a penalty function λ as

$$F = \int_{\text{v}} \left[\nu(\text{Curl}\,\mathbf{A})^2 + \lambda \text{V}(\text{div}\mathbf{A})^2 - 2\mathbf{J}\cdot\mathbf{A}\right] dV \tag{57}$$

Triangular and rectangular prisms are employed for subdividing the field region. The vector potential approximation is defined in terms of the vertex values and weighting functions as

$$\mathbf{A} = \sum \lambda_k \mathbf{A}_k \tag{58}$$

$$\lambda_k = \frac{(a_k + b_k x + C_k y)(1 + r\tau)}{4\Delta} \tag{59}$$

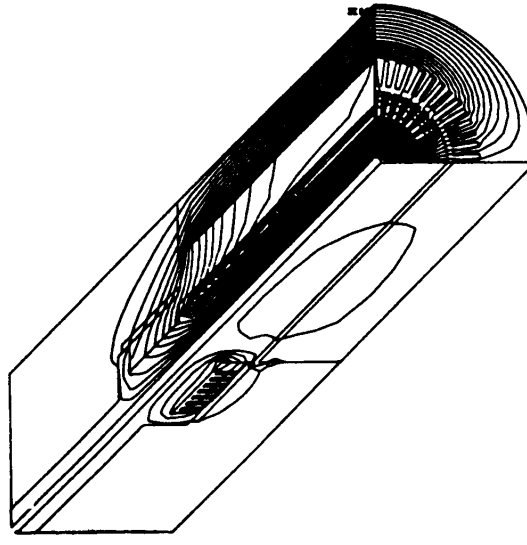

Figure 5.29 No-load field distribution for the 50 MVA generator.

For a first-order triangular prism

$$\lambda_k = \frac{(1+p\xi)(1+q\eta)(1+r\tau)}{2} \tag{60}$$

For a first-order rectangular parallelepiped

a_k, b_k, ξ, η are as described for the 2-dimensional elements.

$\tau = \frac{z}{c}$ where c is the 1/2 length in the Z direction.

r takes a value ± 1 according to the vertex for which the shape function applies.

The solution obtained is applied to an octant of the 50 MVA generator referred to in an earlier section. The equipotential plot of A and vector plot of flux densities are illustrated in Figs. 5.29 and 5.30.

b. Scalar Potential Formulation

We had described earlier two-dimensional finite element solutions for evaluating the magnetic field distribution in permanent magnet machinery. Since magneto- mechanical device topologies are essentially three-dimensional, two-dimensional solutions may not yield the desired accuracy for certain applications.

A three-dimensional field distribution which uses a magnetic scalar potential function may be obtained by using finite element analysis [35].

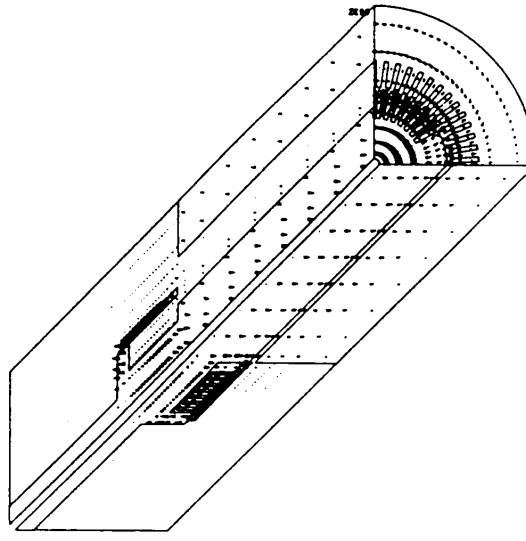

Figure 5.30 No-load vector plot of flux densities for the 50 MVA generator.

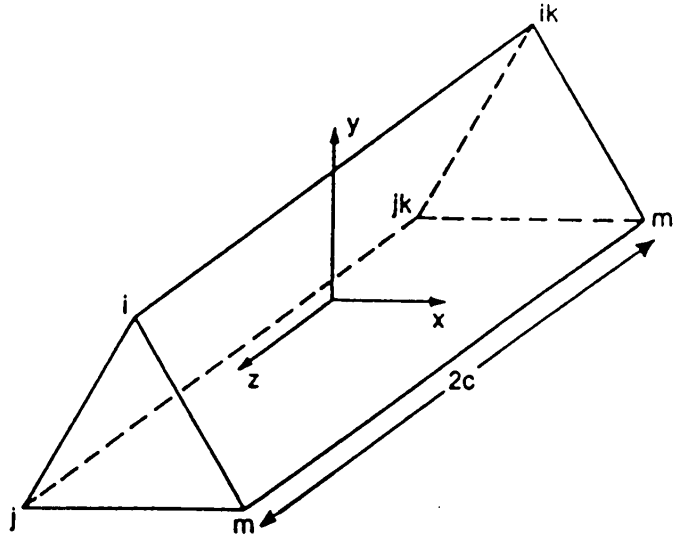

Figure 5.31 Triangular prism element used in discretizing the three-dimensional field region.

The magnetic field distribution in a permanent magnet device can be obtained from the relation described in an earlier section as

$$\frac{\mathbf{B}}{\mu_o} = \mu_r \mathbf{H} + \mathbf{M}_o \tag{61}$$

Taking the divergence of both sides of Eq. (61), and noting that $\mathrm{Div}\mathbf{B} = 0$, there is

$$\mathrm{Div}\mu_r\mu_o\mathbf{H} + \mu_o\mathrm{Div}\mathbf{M}_o = 0 \tag{62}$$

Since $\mathbf{H}$ can be represented by a scalar potential ϕ in

$$\mathbf{H} = -\mathrm{grad}\phi \tag{63}$$

Equation (62) becomes

$$\mathrm{Div}\mu_r\mu_o\mathrm{grad}\phi = \mu_o\mathrm{Div}\mathbf{M}_o \tag{64}$$

Equation (64) is the scalar Poisson Equation for the three-dimensional field problem in terms of the potential function ϕ, the remanent intrinsic magnetization $\mathbf{M}_o$, and the permeability $\mu_r\mu_o$ of the permanent magnet material or ferro-magnetic parts. As for the vector potential case, this equation can be specialized to the different regions as follows.

Source free air-region

$$\mathrm{Div}\,\mathrm{grad}\,\phi = 0 \tag{65}$$

Source free iron particles

$$\mathrm{Div}\,\mu_r\mu_o\mathrm{grad}\,\phi = 0 \tag{66}$$

Permanent magnet region

$$\mathrm{Div}\,\mu_r\mu_o\mathrm{grad}\,\phi = \mu_o\mathrm{Div}\,\mathbf{M}_o \tag{67}$$

Stator current region

$$\mathrm{Div}\,\mathrm{grad}\,\phi = 0 \tag{68}$$

$$\mathrm{grad}\,\phi_1 - \mathrm{grad}\,\phi_2 = \text{sheet current density } \mathbf{J}_s \tag{69}$$

c. *Functional Minimization*

The energy related functional is obtained following the procedure described earlier as

$$F = \int_{\Omega} \mu_r \mu_o (\text{grad}\,\phi)^2 d\Omega + 2\int_{\Omega} \mu_o \phi \text{Div}\,\mathbf{M}_o d\Omega - \oiint_{\Gamma} \phi \mu_r \mu_o \text{grad}\,\phi \cdot d\Gamma \tag{70}$$

For samarium cobalt and ferrite magnets, $\text{Div}\,\mathbf{M}_o$ exists only on the top and bottom pole surfaces. Then the functional reduces to the form

$$F = \int_{\Omega} \mu_r \mu_o (\text{grad}\,\phi)^2 d\Omega - 2\oiint_{\Gamma} \mu_o \mathbf{M}_o \phi \cdot d\Gamma - \oiint_{\Gamma} \phi \mu_r \mu_o \text{grad}\,\phi \cdot d\Gamma \tag{71}$$

Setting the surface integral to zero, yields natural boundary conditions implicit in the functional formulation.

d. *Finite Element Discretization, Shape Functions, and Functional Minimization*

The three-dimensional scalar potential field region may be discretized by triangular prisms shown in Fig. 5.31.

Within each element, the potential function is prescribed in terms of the nodal values and some weighting functions $\zeta_1, \zeta_2 \cdots$ such that

$$\phi = \sum_{i=1,2,\cdots n} \zeta_i \phi_i \tag{72}$$

where

$$\zeta_i = \lambda_i \frac{(1 \pm p\tau)}{2} \tag{73}$$

$$\lambda_i = \frac{(a_i + b_i x + c_i y)}{2\Delta} \tag{74}$$

$$\tau = z/c, \text{and } \Delta \text{ is the triangle area} \tag{75}$$

$$a_i = x_1 y_2 - x_2 y_1 \tag{76}$$

$$b_i = y_2 - y_3 \text{ and } c_i = x_3 - x_2 \text{ in progressive modulo 3} \tag{77}$$

The value of the scalar potential solution is found by minimizing the functional defined by (71), by setting its first variation with respect to the nodal potentials to zero. From (71) one obtains

$$\frac{\partial F}{\partial \phi} = 0 = \iiint_{v} \mu_r \mu_o \nabla \phi \frac{\partial}{\partial \phi_i} \nabla \phi dV - \int_{\Gamma} \mu_o M_o \frac{\partial \phi}{\partial \phi_i} \cdot d\Gamma \tag{78}$$

By substituting $\Sigma\zeta_i\phi_i$ from (72) for ϕ in (78), one obtains

$$\sum_{i=1}^{n} \iiint_{v} \{\mu_r \mu_o [\nabla\zeta_i \cdot \nabla\zeta_j][\phi_i]\}\, dV - \sum_{i=1}^{n} \int_{\Gamma} \mu_o \mathbf{M}_o [\zeta_i] \cdot d\Gamma \qquad (79)$$

The above process is carried out for each of the nodal potentials $\phi_1, \phi_2 \ldots$ for every finite element, and the corresponding matrices are assembled together. The resulting set of equations for all the elements in the entire region reduces to the form

$$[S] \cdot [\phi] = [R] \qquad (80)$$

e. Application to a Disc Machine

The three-dimensional finite element field solution method described above was applied to the disc-type permanent-magnet machine [13] shown in Fig. 5.32. For convenience, the sections over one pole pitch are illustrated. In this instance, it is assumed that the windings are unexcited and carry no current.

Equipotential and vector plots of the scalar potential solution for ϕ are shown in Figs. 5.33 and 5.34. The vector potential solution uses cones for representing the point values in flux-density in magnitude and direction. The flux-density variation along the radial lineover the midplane of the pole and its comparison with tests are illustrated in fig. 5.35.

f. Derivation of Design Constants

This least emphasized area is perhaps the most important one in electrical apparatus design. We shall discuss the evaluation of some of the principal parameters from the vector potential function **A**.

The generated voltage in a conductor is given by

$$V = \omega \oint_{l} \mathbf{A} \cdot dl \qquad (81)$$

The self-inductance may be obtained by determining the total energy stored and dividing the same by the square of the existing current. In the finite-element method, energy is obtained accurately from the expression

$$W = \frac{[A]^T [S][A]}{2} \qquad (82)$$

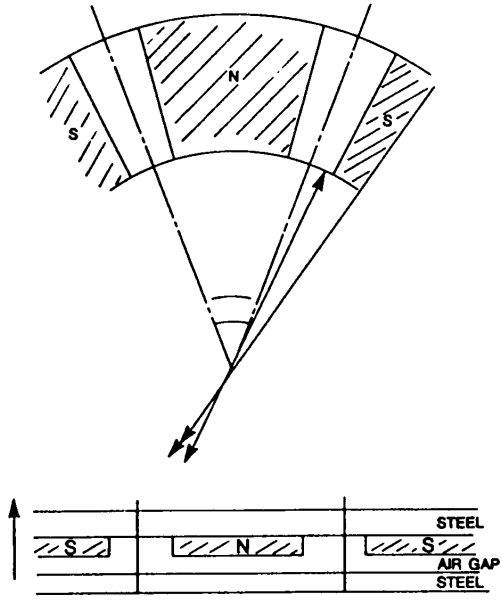

Figure 5.32 Disc permanent magnet machine.

Inductance $L = \frac{W}{I^2}$

Force on a conductor is obtained from the Lorentz force equation

$$F = \int_v \mathbf{J} \times \mathbf{B} dv = \int_v (\mathbf{J} \times \nabla \times \mathbf{A}) dv \tag{83}$$

From the above expression, the torque in a moving element is easily calculated. There are, no doubt, other equally accurate methods of determining forces and torques such as Maxwell's stress tensor, virtual work method, and others.

The losses due to induced currents may be evaluated from the following expression.

$$P = \int_v \frac{J \cdot J^* \rho}{2} dv \tag{84}$$

In the case of electrostatics fields, the electric field and capacitance

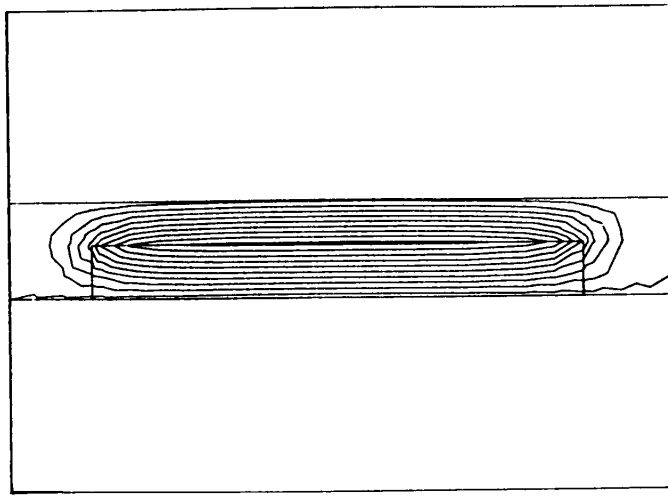

Figure 5.33 Scalar equipotential plot along the radial line over midplane of magnet.

are obtained from the following expressions.

$$E_x = -\frac{\partial V}{\partial x}$$
$$E_y = -\frac{\partial V}{\partial y} \tag{85}$$
$$C = \frac{2[V]^T[S][V]}{V^2}$$

5.5 Conclusion

In this chapter, the finite-element differential equation approach for describing the electromagnetic field distribution in electrical machinery is presented. The application of the method to practical engineering design problems is illustrated. Numerical methods, in general, perform a complementary function to help the design process. It is emphasized that the designer and the analyst pay careful attention to the

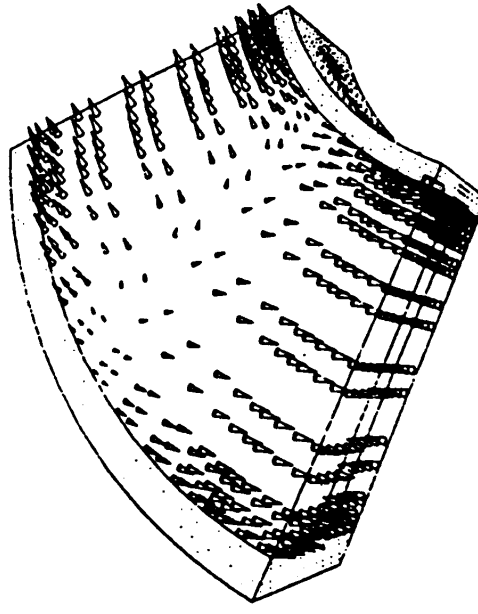

Figure 5.34 Vector plot of flux density over one pole-pitch of the disc machine.

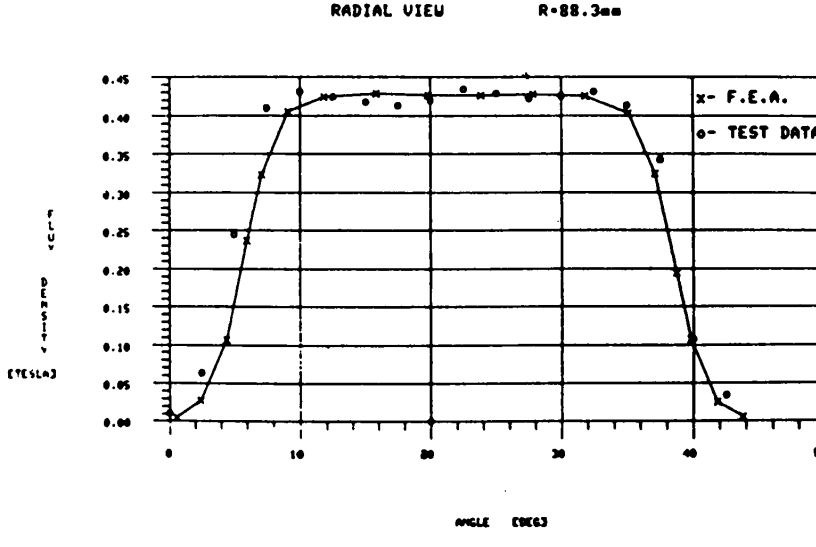

Figure 5.35 Flux-density variation along the radial line over the midplane of the pole.

modeling aspects of the field problem and to the appropriate choice of one or the other of the solution techniques available.

Appendix I. Non-linear Poisson Equation and Functional

Let us consider the curl curl equation:

$$\operatorname{curl} \nu \operatorname{curl} \overline{A} = \overline{J} \tag{1}$$

It is well known in variational calculus that equation (1) can be solved by minimizing the appropriate energy related functional. We might consider the following energy expression

$$W = \frac{1}{2} \int_{\mathrm{v}} \overline{J} \cdot \overline{A} \, dv \tag{2}$$

Rewriting (2), we have

$$W = \int_{\mathrm{v}} \overline{J} \cdot \overline{A} \, dv - \frac{1}{2} \int \overline{J} \cdot \overline{A} \, dv \tag{3}$$

From Ampere's law one has

$$\operatorname{curl} \overline{H} = \overline{J} \tag{4}$$

By the constitutive relationship

$$\overline{H} = \nu \overline{B} \tag{5}$$

And the assumption of a vector potential such that

$$\overline{B} = \nabla \times \overline{A} \tag{6}$$

one obtains by substituting (4), (5) and (6) in (3)

$$W = \int_{\mathrm{v}} \overline{J} \cdot \overline{A} - \frac{1}{2} \int_{\mathrm{v}} \overline{A} \cdot \operatorname{curl} \nu \operatorname{curl} \overline{A} \, dv \tag{7}$$

From vector identities

$$\operatorname{div} (\overline{P} \times \overline{Q}) = \overline{P} \cdot \operatorname{curl} \overline{Q} - \operatorname{curl} \overline{P} \cdot \overline{Q} \tag{8}$$

Substituting

$$\overline{A} \text{ for } \overline{P}; \text{ and } \nu \operatorname{curl} \overline{A} \text{ for } \overline{Q} \text{ in (8)}$$

$$\operatorname{div}\left(\overline{A} \times \nu \operatorname{curl} \overline{A}\right) = \overline{A} \cdot \left(\operatorname{curl} \nu \operatorname{curl} \overline{A}\right) - \left(\operatorname{curl} \overline{A} \cdot \nu \operatorname{curl} \overline{A}\right) \quad (9)$$

From equations (7) and (9), one obtains after some algebraic manipulation and transposition

$$W = \frac{1}{2}\int_{v} \nu(\operatorname{curl} \overline{A} \cdot \operatorname{curl} \overline{A})\, dv + \int_{v} \overline{J} \cdot \overline{A}\, dv + \int \nu \operatorname{div}(\overline{A} \times \nu \operatorname{curl} \overline{A})\, dv \quad (10)$$

For two dimensional magnetostatic fields with a single 'z' directed component of vector potential, there is, in cartesian coordinates

$$\operatorname{curl} \overline{A} = \frac{\partial A}{\partial y}\hat{i} - \frac{\partial A}{\partial x}\hat{j}$$

One can, therefore, write

$$\operatorname{curl} \overline{A} \cdot \operatorname{curl} \overline{A} = \left(\frac{\partial A}{\partial x}\right)^2 + \left(\frac{\partial A}{\partial y}\right)^2$$

and

$$\overline{A} \times \nu \operatorname{curl} \overline{A} = A\frac{\partial A}{\partial y}\hat{j} + A\frac{\partial A}{\partial x}\hat{i} = A\frac{\partial A}{\partial n} \cdot \hat{n} \quad (11)$$

substituting the results of (11) and (10) and after converting the last of the integral into a surface integral by divergence theorem, one obtains the functional expression for (2) as

$$W = \frac{1}{2}\int_{v} \nu \left\{ \left(\frac{\partial A}{\partial x}\right)^2 + \left(\frac{\partial A}{\partial y}\right)^2 \right\} dv - \int_{v} \overline{J} \cdot \overline{A}\, dv + \oint_{\Gamma} A\frac{\partial A}{\partial n} d\Gamma \quad (12)$$

We have yet to show that the minimization of (12) yields the required vector potential solution that satisfies the differential equation (1). It is shown in reference [21] and in text books of variational calculus, that if the Euler equation to (12) yields the differential equation (1), then $\overline{A}$ satisfies the differential equation.

The Euler equation may be written as

$$\frac{\partial}{\partial x}\left(\frac{\partial F}{\partial Ax}\right) + \frac{\partial F}{\partial y}\left(\frac{\partial F}{\partial Ay}\right) - \frac{\partial F}{\partial A} = 0 \quad (13)$$

Where F is the integrand of the first two volume integrals in (12) and

$$Ax = \frac{\partial A}{\partial x}; \quad Ay = \frac{\partial A}{\partial y} \tag{14}$$

Now

$$F = \frac{\nu}{2}\left[\left(\frac{\partial A}{\partial x}\right)^2 + \left(\frac{\partial A}{\partial y}\right)^2\right] - \overline{J} \cdot \overline{A} \tag{15}$$

Therefore

$$\frac{\partial F}{\partial Ax} = \nu\left(\frac{\partial A}{\partial x}\right); \frac{\partial F}{\partial Ay} = \nu\left(\frac{\partial A}{\partial y}\right); \text{ and } -\frac{\partial F}{\partial A} = \overline{J} \tag{16}$$

Substituting the results of (16) in (13), we have

$$\frac{\partial}{\partial x}\nu\left(\frac{\partial A}{\partial x}\right) + \frac{\partial}{\partial y}\nu\left(\frac{\partial A}{\partial y}\right) + J = 0 \tag{17}$$

If we expand equation (1) in two-dimensional cartesian coordinates and know that both $\overline{A}$ and $\overline{J}$ have only unidirectional 'z' directed components

$$\left(\frac{\partial}{\partial x}\hat{i} + \frac{\partial}{\partial y}\hat{j}\right)\nu \times \left(\frac{\partial A}{\partial y}\hat{i} - \frac{\partial A}{\partial x}\hat{j}\right) = \overline{J} \tag{18}$$

or

$$-\frac{\partial}{\partial x}\nu\left(\frac{\partial A}{\partial x}\right)\hat{k} - \frac{\partial}{\partial y}\nu\left(\frac{\partial A}{\partial y}\right)\hat{k} = J\hat{k} \tag{19}$$

Rewriting (19) and dropping $\hat{k}$ throughout

$$\frac{\partial}{\partial x}\nu\left(\frac{\partial A}{\partial x}\right) + \frac{\partial}{\partial y}\nu\left(\frac{\partial A}{\partial y}\right) + J = 0 \tag{20}$$

We observe (17) and (20) are identical and conclude that the functional expression of (10) is the required functional. Now let us examine equation (10). Since

$$\overline{B} = \text{curl}\,\overline{A}$$

the first term represents the stored magnetic energy.

$$W = \frac{1}{2}\int_v \nu\overline{B} \cdot \overline{B}dv \tag{21}$$

For a general nonlinear case, the integrand $f = \nu \overline{B} \cdot \overline{B}/2$ of (21) can be written as $\int_0^B \nu B dB$ so that (21) becomes

$$W = \int_v \left[\int_o^B \nu B dB \right] dv \tag{22}$$

Therefore, we may rewrite the functional expression for the nonlinear magnetostatic problem as

$$W = \int_v \left[\int_o^B \nu B dB \right] dv - \int_v \overline{J} \cdot \overline{A}\, dv - \oint_\Gamma A \frac{\partial A}{\partial n} d\Gamma \tag{23}$$

Boundary Conditions

Now let us examine the surface integral term. If there is no variation in A such as by specifying a zero or a constant potential, the surface integral can be set to zero since its derivative with respect to each A_k will be zero. This is called a flux tangential boundary condition or in general the 'Dirichlet' boundary condition. If on the other hand we set the boundary integral to zero even if A is not zero or a constant, then it will necessarily meant that $\frac{\partial A}{\partial n} = 0$. This corresponds to a flux normal boundary or in general terms called the Homogeneous Neumann boundary condition.

Appendix II. Functional for the Eddy Current Problem in Conductors with Eddy Current Free Source

$$W = \frac{1}{2} \int \overline{J}^* \cdot \overline{A}\, dv + \frac{1}{2} \int \overline{J} \cdot \overline{A}^* dv \tag{1}$$

Now

$$\overline{J} = \overline{J}_e + \overline{J}_s \tag{2}$$

Where J_s is the source current density and $\overline{J}_e$ the eddy current density. From the 2nd Maxwell's equation (Faraday's law of induction) for time harmonic fields and with the assumption $\overline{B} = \operatorname{curl} \overline{A}$.

$$\operatorname{Curl} \overline{\mathrm{E}} = -\mathrm{j}\omega \overline{\mathrm{B}} = -\mathrm{j}\omega \operatorname{curl} \overline{\mathrm{A}} \tag{3}$$

Therefore dropping the curl's on both sides of the equation (3) one obtains

$$\overline{E} = -j\omega \overline{A} \tag{4}$$

Using Ohm's law we have

$$J_e = \sigma E = -j\omega\sigma A \tag{5}$$

Substituting (5) in (2) and the result in (1), one obtains for the eddy current part of the functional

$$W_e = \frac{1}{2}\int -j\omega\sigma\overline{A}^* \cdot \overline{A}\, dv + \frac{1}{2}\int -j\omega\sigma\overline{A} \cdot \overline{A}^* dv \tag{6}$$

$$= \int -j\omega\sigma\overline{A} \cdot \overline{A}^* dv \tag{7}$$

Now for the non-eddy current region where $\overline{J}_e = 0$, as in the case of magnetostatic analysis and following the same procedure one can obtain the functional for the linear case as

$$W_s = -\int_v \frac{\nu}{2}(\operatorname{curl}\overline{A}^*) \cdot (\operatorname{curl}\overline{A})\, dv + \int 2\overline{J}_s^* \cdot \overline{A}\, dv + \int_v \frac{\nu}{2}(\operatorname{curl} A) \cdot (\operatorname{curl} A^*) dv + \int 2\overline{J} \cdot \overline{A}^* dv \tag{8}$$

Since $W = W_e U W_s$ we have

$$W = -\int_v \nu(\operatorname{curl}\overline{A}) \cdot (\operatorname{curl} A^*) dv - \int j\omega\sigma\overline{A} \cdot \overline{A}^* dv + \int 2\overline{J}_s^* \cdot \overline{A}\, dv + \int 2\overline{J}_s \cdot \overline{A}^* dv \tag{9}$$

Minimization of W with respect to each nodal value of A_k yields

$$\frac{\partial W}{\partial A_k^*} = -\int_v \nu(\operatorname{curl}\overline{A})\frac{\partial}{\partial A_k^*}(\operatorname{curl}\overline{A}^*) dv - \int j\omega\sigma\overline{A} \cdot \frac{\partial}{\partial A_k^*}\overline{A}^* dv + \int 2\overline{J}_s \cdot \frac{\partial}{\partial A_k^*}\overline{A}^* dv = 0 \tag{10}$$

Similarly

$$\frac{\partial W}{\partial A_k} = -\int_v \nu(\operatorname{curl}\overline{A}^*)\frac{\partial}{\partial A_k}(\operatorname{curl} A)\, dv - \int j\omega\sigma\overline{A}^* \cdot \frac{\partial}{\partial A_k}\overline{A}\, dv + \int 2\overline{J}_s^* \frac{\partial}{\partial A_k}\overline{A}\, dv \tag{11}$$

Equation (10) will result in a symmetric matrix in terms of $\overline{A}$ and $\overline{J}_s$ free of conjugate terms such as $\overline{A}^*$ and $\overline{J}_s^*$. Similarly (11) will be free of $\overline{A}$ and $\overline{J}_s$ and therefore their coefficient matrices will be identical and one may solve for $\overline{A}$ or $\overline{A}^*$ with the appropriate source term. Without any loss of generality we can write the functional with new variables Ψ and Φ (so called Galerkin Functional) which when minimized would yield the same coefficient matrices as (10) or (11).

$$W = -\int \nu(\operatorname{curl}\Psi)\cdot(\operatorname{curl}\Psi)\,dv - \int jw\sigma\Psi\cdot\Psi\,dv + \int 2\Phi_s\cdot\Psi\,dv \quad (12)$$

When Ψ can be either $\overline{A}$ or $\overline{A}^*$ and Φ can be J_s or $\overline{J}_s^*$.

Also for two-dimensional problems $(\operatorname{curl}\Psi\cdot\operatorname{curl}\Psi)$ is identically the same as $(\operatorname{grad}\Psi\cdot\operatorname{grad}\Psi)$ and hence (12) reduces to the form

$$W = +\iint \left[(\nu\operatorname{grad}\Psi)^2 + jw\sigma\Psi\cdot\Psi - 2\Phi_s\cdot\Psi\right] dxdy \quad (13)$$

If we substitute back $\overline{A}$ for Ψ and J_s for Φ_s one obtains the functional as

$$W = \iint \left[\nu\left(\operatorname{grad}\overline{A}\right)^2 + j\Psi\sigma\overline{A}\cdot\overline{A} - 2\overline{J}_s\cdot\overline{A}\right] dxdy \quad (14)$$

Equation (14) is identically the same as equation (32) in the text.

References

[1] Carter, G. W., *The Electromagnetic Field in its Engineering Aspects*, Longmans Green and Co., London, 1954.

[2] Tozoni, O. V., *Mathematical Models for the Evaluation of Electric and Magnetic Fields*, Iliffe Books Ltd., London, 1968.

[3] Fuchs, E. F., and E. A. Erdelyi, "Nonlinear theory of turboaltenators," *Parts I and II, IEEE Trans.*, **PAS-92** No. 2, 533–592, 1974.

[4] Csendes, Z. J., "The high order polynomial finite element method in electromagnetic field computation," *Finite Elements in Electrical and Magnetic Field Problems*, **Chapter 7**, John Wiley and Sons, Ltd., U.K., 1980.

[5] Silvester, P., and M. V. K. Chari, "Finite element solution of saturable magnetic field problems," *IEEE Trans.* **PAS-89,** No. 7, 1642–1651, 1970.

[6] Simkin, J., and C. W. Trowbridge, "Application of integral equation methods for the numerical solution of magnetostatic and eddy current problems," *Rutherford Laboratory Report,* **RL-76-041,** U.K.

[7] "Improvement in accuracy of prediction of electrical machine constants," *EPRI final Report,* **2,** Apr. 1984.

[8] Minnich, S. H., Z. J. Csendes, M. V. K. Chari, S. C. Tandon, and J. F. Berkery, "Load characteristics of synchronous generators by the finite element method," *IEEE PES,* **F-80,** 206–3, Winter Meeting, 1980.

[9] Konrad, A., and M. V. K. Chari, "Power loss and forces due to skin effect in transmission lines and busbars," *IEEE Canadian Communications and Energy Conference,* Oct. 13-15, Montreal 1982.

[10] Dimonaco, A., G. Giuseppetti, and G. Tontini, "Studio di campi elettrici e magnetici stanzionari con II metodo degli elementi finiti applicazione ai transformatori," *Lèlettotecnica,* **LXII,** No. 7, 585–598., 1975.

[11] Tandon, S. C., "Finite element analysis of induction machines," *IEEE Trans. Magnetics,* **MAG-18,** No. 6, 1722–1724, Nov. 1982.

[12] Chari, M. V. K., and P. Silvester, "Finite element analysis of magnetically saturated DC machines," *IEEE Paper 71,* **IP3-PWR** Winter Meeting, Feb. 1971.

[13] Chari, M. V. K., and J. D'Angelo, "Finite element analysis of magneto-mechanical devices," *Proceedings of the Fifth International Workshop on Rare Earth Cobalt Magnets and Their Applications,* Roanoke, Virginia, 237–257, June 7-10, 1981.

[14] Kincaid, T. G., and M. V. K. Chari, "The application of finite element analysis method to eddy current nondestructive evaluation," *IEEE Trans.,* **MAG-15,** No. 6, 1956–1960, 1979.

[15] Palmo, M. A., Z. J. Csendes, and M. V. K. Chari, "Axisymmetric and three dimensional electrostatic field solutions by the finite element method," *Electrical Machines & Electromechanics,* Quar-

terly, 235–244, 1979.

[16] Silvester, P., H. S. Cabayan, and B. T. Browne, "Efficient techniques for finite element analysis of electric machines," *IEEE Trans.*, **PAS – 9^{TM}**, No. 4, 1973.

[17] Cuthill, E. H., and J. M. McKee, "Reducing the bandwidth of sparse symmetric matrices," *Proc. 24th Conference SCM,* 157–172, 1969.

[18] Bathe, K. J., and E. L. Wilson, *Numerical Methods in Finite Element Analysis,* Prentice Hall, Englewood Cliffs, N.J. 1976.

[19] Irons, B. M., "A frontal solution program for finite element analysis," *Int. J. of Num. Methods in Engineering.,* **2,** 5–32, 1970.

[20] Hestenes, M. R., and E. Stiefel, "Method of conjugate gradients for solving linear systems," Report No. 1959, NBS, Washington, D.C. 1952.

[21] Chari, M. V. K., "Finite element analysis of nonlinear magnetic fields in electric machines," *PhD. Dissertation,* McGill University, Montreal, Canada 1970.

[22] Brandl, P., K. Reichert, and W. Vogt, "Simulation of turbogenerators on steady state load," *Brown Boveri Review,* **9,** 1975.

[23] Bedrosian, G., M. V. K. Chari, M. R. Shah, and G. Theodossiou, "Axiperiodic finite element analysis of generator end regions; Part I-Theory," *IEEE Trans. Magnetics,* July 1989.

[24] Hildebrand, F. B., *Modern Mathematics for Engineers and Physicists,* Prentice Hall, Englewood Cliffs, N.J. 1962

[25] Honsinger, V. B., "Permanent magnet AC motors," *Presentation to Industry Application Society, IEEE,* Nov. 1980.

[26] Chari, M. V. K., E. T. Laskaris, and J. D'Angelo, "Finite element analysis of a magnetic fluid seal for large-diameter high-speed rotating shafts," *Intermag Conference,* **21-7,** Grenoble, 1981.

[27] Jackson, J. D., *Classical Electrodynamics,* John Wiley and Sons, New York 1962.

[28] Silvester, P., and C. R. S. Haslam, "Magnetotelluric modeling by the finite element method," *Geophysical Prospecting,* **20,** 872–891, 1972.

[29] Chari, M. V. K., "Finite element solution of the eddy-current problem in magnetic structures," *IEEE Trans.*, **PAS-93**, No. 1, 1973.

[30] Minnich, S. H., J. W. Dougherty, and D. K. Sharma, "Calculation of generator simulation-model constants using finite element analysis," *ICEM*, Budapest, Hungary, Sept. 1982.

[31] Donea, J., S. Giuliani, and A. Philippe, "Finite elements in the solution of electromagnetic induction problems," *Int. J. of Num. Methods in engineering*, **8**, 359–367, 1974.

[32] Foggia, A., J. C. Sabonnadiere, and P. Silvester, "Finite element solution of saturated traveling magnetic field problems," *IEEE Trans.*, **PAS-94**, No. 3, 1975.

[33] Csendes, Z. J., and M. V. K. Chari, "General finite element analysis of rotating electric machines," *International Conference on Numerical Methods in Electrical and Magnetic Field Problems*, St. Margherita, Italy 1976.

[34] Minnich, S. H., "Incremental permeabilities for transient analysis of large turbine generators by the finite element method," *J. of Applied Physics*, **52(3)**, 2428–2430, Mar. 1981.

[35] Chari, M. V. K., "Finite element analysis of electrical machinery and devices (invited)," *IEEE Trans. on Magnetics*, **MAG-16**, No. 5, Sept. 1969.